

This work is licensed under a Creative Commons Attribution License (CC BY 4.0).

Research article

urn:lsid:zoobank.org:pub:F96F56AC-158A-400C-A096-ABF06D8C21C0

Neanthes goodayi sp. nov. (Annelida, Nereididae), a remarkable new annelid species living inside deep-sea polymetallic nodules

Regan DRENNAN^{1,*}, Helena WIKLUND², Muriel RABONE³,
Magdalena N. GEORGIEVA⁴, Thomas G. DAHLGREN⁵ & Adrian G. GLOVER⁶

¹ Ocean & Earth Science, University of Southampton, European Way, Southampton SO14 3ZH, UK.

^{1,2,3,4,6} Life Sciences Department, Natural History Museum, London SW7 5BD, UK 2.

^{2,5} Department of Marine Sciences, University of Gothenburg, Box 463, 40530 Gothenburg, Sweden.

^{2,5} Gothenburg Global Biodiversity Centre, Box 463, 40530 Gothenburg, Sweden.

⁵ NORCE Norwegian Research Centre, Bergen, Norway.

* Corresponding author: r.drennan@nhm.ac.uk

² Email: helena.wiklund@marine.gu.se

³ Email: M.Rabone@nhm.ac.uk

⁴ Email: m.georgieva@nhm.ac.uk

⁵ Email: thda@norceresearch.no

⁶ Email: a.glover@nhm.ac.uk

¹ urn:lsid:zoobank.org:author:63A79724-B7EC-4D7D-99BF-2B3CB2EBCD6D

² urn:lsid:zoobank.org:author:114C3853-7E48-42AC-88F3-F7AC327B24F3

³ urn:lsid:zoobank.org:author:0D08F91D-A967-4A8B-A244-9963239F044A

⁴ urn:lsid:zoobank.org:author:76E89A87-2986-4574-895E-2FFF0743CDD6

⁵ urn:lsid:zoobank.org:author:B24FC764-1770-41EA-8CF8-E1CDD0C4E489

⁶ urn:lsid:zoobank.org:author:03878173-9B00-462A-98BC-4E246E3D32FF

Abstract. A new species of abyssal *Neanthes* Kinberg, 1865, *N. goodayi* sp. nov., is described from the Clarion-Clipperton Zone in the central Pacific Ocean, a region targeted for seabed mineral exploration for polymetallic nodules. It is a relatively large animal found living inside polymetallic nodules and in xenophyophores (giant Foraminifera) growing on nodules, highlighting the importance of the mineral resource itself as a distinct microhabitat. *Neanthes goodayi* sp. nov. can be distinguished from its congeners primarily by its distinctive, enlarged anterior pair of eyes in addition to characters of the head, pharynx and parapodia. Widespread, abundant, and easily recognisable, *N. goodayi* sp. nov. is also considered to be a suitable candidate as a potential indicator taxon for future monitoring of the impacts of seabed mining.

Keywords. CCZ, molecular phylogeny, Polychaeta, morphology, abyssal fauna.

Drennan R., Wiklund H., Rabone M., Georgieva M.N., Dahlgren T.G. & Glover A.G. 2021. *Neanthes goodayi* sp. nov. (Annelida, Nereididae), a remarkable new annelid species living inside deep-sea polymetallic nodules. *European Journal of Taxonomy* 760: 160–185. <https://doi.org/10.5852/ejt.2021.760.1447>

Introduction

Exploration of our deep oceans for potential new industrial activities has increased rapidly in recent decades with the so-called ‘blue growth’ economy (European Commission 2020). Critical to a sustainable blue economy is baseline knowledge on the environmental characteristics of these exploration areas, in particular knowledge of the species that live there (Glover *et al.* 2018). This is especially the case in the central Pacific abyss Clarion-Clipperton Zone (CCZ), a region targeted for seabed mineral exploration for polymetallic nodules, where basic faunistic and taxonomic data are notably lacking and many animals likely undescribed or undocumented (Glover *et al.* 2018). Here, we describe a new nereidid annelid from the abyss that is not only important for understanding the general baseline biology of the region, but also presents a remarkable natural history – living inside the polymetallic nodules themselves. As the species is relatively large and easy to recognise, it should be added to a list of nodule-dwelling fauna that could be used as indicators in future environmental assessments (Lim *et al.* 2017). Information on the existence, abundance and distribution of these species could be essential to environmental monitoring and conservation measures in the region.

The CCZ lies in international waters and lacks strictly defined boundaries; however, it is generally accepted to encompass the region between the Clarion and Clipperton Fracture Zones, with multiple polymetallic nodule exploration contracts for seabed minerals issued by the International Seabed Authority (ISA 2018), extending from 115° W (the easternmost extent of the UK-1 polymetallic nodule exploration area) to approximately 158° W (the westernmost extent of the COMRA polymetallic nodule exploration area). As such, we hereafter use a working definition of the CCZ as comprising the box: 13° N, 158° W; 18° N, 118° W; 10° N, 112° W; 2° N, 155° W – an area spanning almost 6 million km², approximately 1.4% of the ocean’s surface.

Polymetallic nodules are small mineral accretions (usually 5–10 cm in diameter, but occasionally exceeding 20 cm) rich in cobalt, manganese, copper and nickel, among numerous other metals of economic interest (Hein *et al.* 2013). These nodules sit on the sea floor, often half submerged in sediment, providing the only hard substrate in an otherwise soft sediment environment, contributing to a high habitat heterogeneity compared with regions of the deep sea without nodules or hard substrate. Nodules provide microhabitats for meio- and macrofaunal groups such as annelids and crustaceans (Thiel *et al.* 1993; Gooday *et al.* 2017; Kersken *et al.* 2019), in addition to sites of attachment for sessile megafauna (e.g., *Relicanthus* sp. anemones) (Amon *et al.* 2016).

Nereididae de Blainville, 1818 is among the most diverse families within Annelida, with over 40 valid genera and up to 750 valid species (Read & Fauchald 2020a). Members of the family are broadly omnivorous, and most species appear to be facultatively motile, rarely leaving mucus-built tubes and burrows unless disturbed or when conditions become unfavourable (Fauchald & Jumars 1979; Jumars *et al.* 2015). Sexually mature individuals may develop into pelagic morphs (epitokes), which are thought to have much greater motility. However, not all nereidids form epitokes during reproduction, and not all epitokes are pelagic, with the degree of modification varying between species and sexes (Bakken & Wilson 2005).

The genus *Neanthes* Kinberg, 1865 is one of the most diverse genera within the family, with over 80 currently accepted species (Read & Fauchald 2020b), and can be distinguished from similar genera such as *Hediste* Malmgren, 1867 and *Nereis* Linnaeus, 1758 by morphological characters primarily relating to the presence or absence of certain chaetal types, for example in lacking compound falcigers in notopodial fascicles (as in *Nereis*), but possessing homogomph spinigers in ventral neuropodial fascicles (absent in *Hediste* and *Nereis*) (Bakken & Wilson 2005).

However, *Neanthes* is considered to be polyphyletic (Bakken & Wilson 2005) and a generic revision based on phylogenetic analyses is needed to resolve its taxonomy (Bakken & Wilson 2005; Bakken 2006; Glasby *et al.* 2011; Shimabukuro *et al.* 2017; Villalobos-Guerrero 2019). The majority of species of *Neanthes* have been described from shallow or intertidal waters, with only 13 species reported from depths greater than 200 m (Khlebovich 1996; Shimabukuro *et al.* 2017; Hsueh 2019). Notably, Thiel *et al.* (1993), when examining nodules collected from the South Pacific (outside of the CCZ) as part of the DISCOL project, reported two unidentified species of *Neanthes* when first describing polymetallic nodule crevices as a discrete microhabitat; these were among six annelid taxa that were only found within interstitial mud from nodule crevices, and not from the surrounding soft sediment.

In this study, we describe a new species of abyssal *Neanthes* observed to reside either directly within nodule crevices, within mud balls on nodule surfaces or burrowing within xenophyophores (giant foraminiferans) growing on nodules. This species is notable in that it highlights the potential importance of nodule microhabitats for macrofaunal-sized animals, and is also one of the most abundant and widespread annelid species collected as part of the ABYSSLINE ('ABYSSal baseLINE') UK-1 environmental survey project. Easily recognisable, it is a critical 'target taxon' for further assessments of biogeography and population connectivity patterns, the subject of a separate study (Dahlgren *et al.*, unpublished data).

Material and methods

Fieldwork

Specimens were collected across two cruises, the first UK Seabed Resources ABYSSLINE cruise (AB01) sampling the UK-1 exploration contract area aboard the RV *Melville*, October 2013, and the second cruise (AB02) sampling the UK-1 and OMS (Ocean Mineral Singapore) exploration contract areas as well as an area to the north designated as Area of Particular Environmental Interest 6 (APEI-6) onboard RV *Thomas G. Thompson*, February–March 2015 (Fig. 1). A comprehensive description of the DNA taxonomy methodological pipeline used here is provided in Glover *et al.* (2016). In summary, a range of oceanographic sampling gear, including box corer, epibenthic sledge (EBS), ROV and multiple corer, were used to collect deep-sea benthic specimens from the UK-1, OMS and APEI-6 areas. Geographic data from sampling activities were recorded on a central GIS database. A 'cold-chain' pipeline was used in the live-sorting of specimen samples aboard both vessels, where material was constantly maintained in chilled, filtered seawater held at 2–4 °C. Specimens underwent preliminary identification at sea and were live-imaged using digital cameras attached to stereo microscopes (Glover *et al.* 2016). All specimens were then stored in individual microtube vials containing an aqueous solution of 80% non-denatured pre-chilled ethanol, which were numbered, barcoded into a database and stored chilled until return to the Natural History Museum, London, UK.

Laboratory work

A total of 43 specimens were identified as conspecific using genetic data (see below) and considered in morphological analyses, with a portion of representative specimens selected as type material for more detailed analyses.

Specimen measurements taken included total length (TL), length to chaetiger 15 (L15), width of chaetiger 15 excluding parapodia (W15), and the total number of chaetigers for complete specimens. Paragnaths for each pharangeal area were counted, with paired areas that differed in numbers distinguished using *a* and *b* for the left and right side of the specimen respectively. The number of teeth on the jaws were also counted. For specimens where the pharynx was not everted, a longitudinal dissection was made in the mid-ventral region. For examination of parapodial features and modifications along the body, several

parapodia were removed (from chaetigers 1, 3, 6, 10, every tenth chaetiger thereafter, and a posterior-most chaetiger, where possible) and mounted on glass slides. Parapodia were dissected from either the left or right side of the specimen based on intactness of features such as cirri.

Specimens were examined using compound and light microscopes, and photographed using attached digital cameras on both microscopes. Figures were assembled using Adobe Photoshop CS6 software. A fine white or black line was used to outline and highlight particular morphological features where they were unclear from the images alone. Standardised terminology of nereidid parapodial features follows Villalobos-Guerrero & Bakken (2018); the shape of pharyngeal areas and ridge patterns follows Villalobos-Guerrero (2019).

A small tissue sample was taken from each specimen for DNA extraction. The DNeasy Blood and Tissue Kit (Qiagen) was used to extract DNA using a Hamilton Microlab STAR Robotic Workstation. Approximately 1800 bp of 18S rRNA (18S) were amplified using the primers 18SA 5'-AYCTGGTTGATCCTGCCAGT-3'

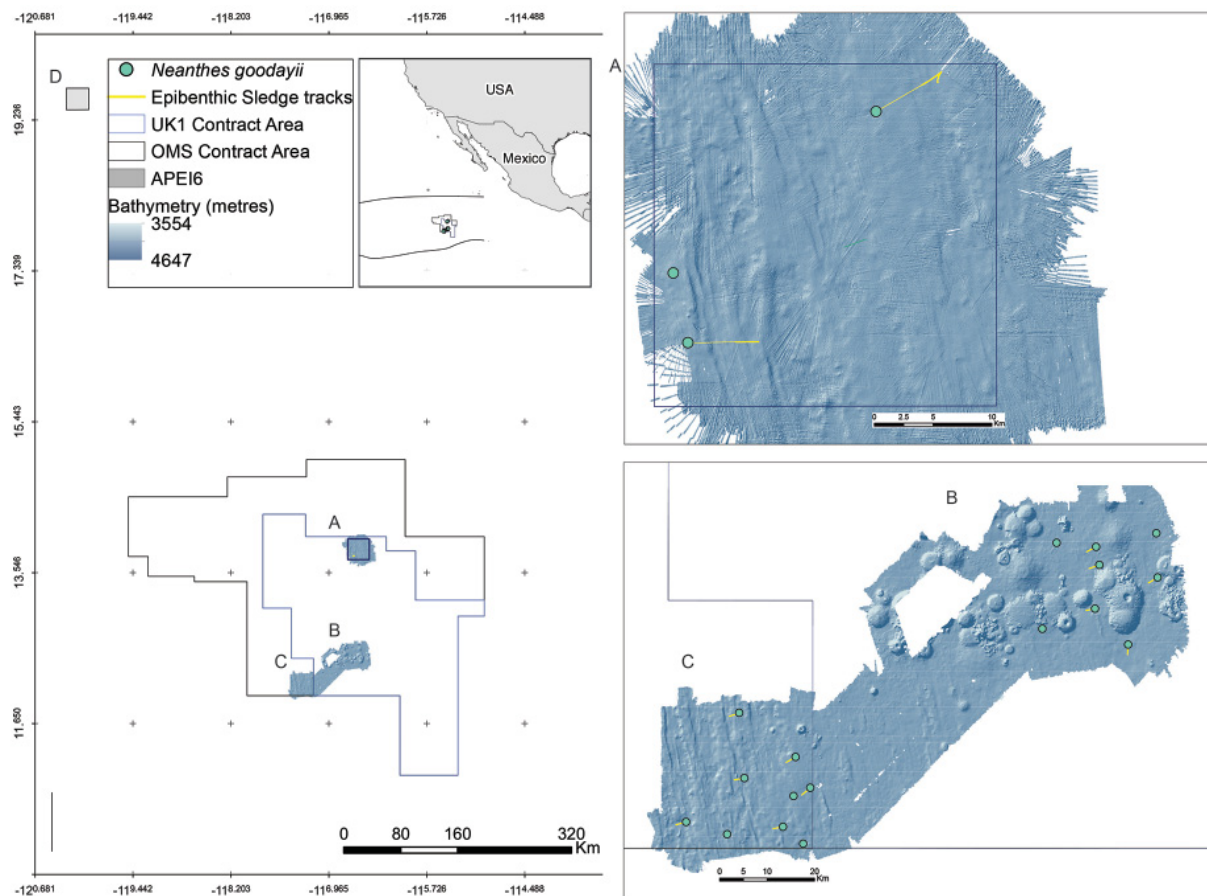


Fig. 1. Sampling sites, showing occurrences of *Neanthes goodayii* sp. nov. **A.** UK-1 Stratum-A study area within the UK Seabed Resources UK-1 exploration contract area. **B.** UK-1 Stratum-B study area within the UK Seabed Resources UK-1 exploration contract area. **C.** OMS Stratum-A study area, in the Ocean Mineral Singapore (OMS) polymetallic nodule exploration contract area. **D.** Area of Particular Environmental Interest APEI-6. Inset map showing location of Clarion-Clipperton Fracture Zone in the Central Eastern Pacific. Bathymetric survey data and sampling localities from the AB01 2013 RV *Melville* survey cruise (MV1313) and AB02 2015 RV *Thomas G. Thompson* survey cruise (TN319); data courtesy of Craig R. Smith (University of Hawaii), UK Seabed Resources Ltd. and Seafloor Investigations, LLC.

Table 1. List of taxa used in phylogenetic analyses with respective NCBI GenBank accession numbers.

Taxon name	GenBank accession numbers		
	18S	16S	COI
<i>Alitta succinea</i> (Leuckart, 1847)	AY210447	KT959483	KT959389
<i>Alitta virens</i> (M. Sars, 1835)	Z83754	–	AF221572
<i>Ceratocephale abyssorum</i> (Hartman & Fauchald, 1971)	GQ426585	GQ426618	–
<i>Ceratocephale loveni</i> Malmgren, 1867	DQ442616	DQ442614	–
<i>Ceratonereis longiceratophora</i> Hartmann-Schröder, 1985	AB106251	–	AY583701
<i>Dendronereis aestuarina</i> Southern, 1921	KT900288	–	–
<i>Dendronereis</i> sp. (CUGD1)	KF586536	–	–
<i>Dendronereis</i> sp. (CUGD2)	KF586537	–	–
<i>Hediste atoka</i> Sato & Nakashima, 2003	LC323073	AB703090	AB603842
<i>Hediste diadroma</i> Sato & Nakashima, 2003	LC323646	LC323062	–
<i>Hediste diversicolor</i> (O.F. Müller, 1776)	LC381864	LC323090	KR916844
<i>Hediste japonica</i> (Izuka, 1908)	LC323647	LC323064	AB603758
<i>Hediste limnicola</i> (Johnson, 1903)	LC381865	LC323068	–
<i>Namalycastis abiuma</i> group sp. MM-2010	HQ157237	HM138705	JQ081269
<i>Namalycastis hawaiiensis</i> (Johnson, 1903)	LC213729	LC213728	–
<i>Namalycastis jaya</i> Magesh <i>et al.</i> , 2012	HQ157238	HM138706	HQ456363
<i>Neanthes goodayi</i> sp. nov. (NHM_171)	MZ408643	MZ408646	MZ407911
<i>Neanthes goodayi</i> sp. nov. (NHM_173)	MZ408644	MZ408647	MZ407912
<i>Neanthes acuminata</i> isolate ABF1	–	KJ538978	KJ539071
<i>Neanthes acuminata</i> isolate LAF1	–	KJ538984	KJ539083
<i>Neanthes acuminata</i> isolate NPF5	–	KJ538994	KJ539092
<i>Neanthes acuminata</i> isolate POF6	–	KJ538966	KJ539101
<i>Neanthes acuminata</i> isolate VLF1	–	KJ538969	KJ539128
<i>Neanthes</i> cf. <i>glandicineta</i> (Southern, 1921)	–	LC323071	LC323035
<i>Neanthes fucata</i> (Savigny, 1822)	–	–	KR916874
<i>Neanthes meggitti</i> (Monro, 1931)	–	MF959006	MF958994
<i>Neanthes shinkai</i> Shimabukuro <i>et al.</i> , 2017	–	–	LC331618
<i>Neanthes</i> sp. LH-2011	–	–	JF293305
<i>Neanthes wilsonchani</i> Lee & Glasby, 2015	–	MF850380	MG251655
<i>Nectoneanthes oxyroda</i> (Marenzeller, 1879)	KX290701	–	–
<i>Neogyptis carriebowcayi</i> Pleijel <i>et al.</i> , 2012	JN631338	JN631325	JN631315
<i>Neogyptis fauchaldi</i> Pleijel <i>et al.</i> , 2012	JN631339	JN631326	JN631316
<i>Neogyptis hinehina</i> Pleijel <i>et al.</i> , 2012	JN631340	JN631328	JN631317
Nereididae sp. (MB-2010)	GQ426586	–	–
<i>Nereis heterocirrata</i> Treadwell, 1931	KC840697	KC833487	GU362684
<i>Nereis pelagica</i> Linnaeus, 1758	AF474279	AY340470	HM473499
<i>Nereis sandersi</i> Blake, 1985	AM159579	–	–
<i>Nereis vexillosa</i> Grube, 1851	DQ790083	GU362677	HM473511
<i>Perinereis aibuhitensis</i> (Grube, 1878)	KC840692	KC833485	JX503021
<i>Perinereis cultrifera</i> (Grube, 1840)	KJ182978	KC833495	KR916911
<i>Perinereis mictodonta</i> (Marenzeller, 1879)	–	KC833496	KC800632
<i>Perinereis nuntia</i> (Lamarck, 1818)	–	LC482156	MH337359
<i>Perinereis wilsoni</i> Glasby & Hsieh, 2006	KC840691	KC833494	KC800623
<i>Platynereis australis</i> (Schmarda, 1861)	KT900290	–	–
<i>Platynereis dumerilii</i> (Audouin & Milne Edwards, 1833)	AY894303	KP640622	KC591838
<i>Pseudonereis</i> sp. (pse179)	KT900283	–	–
<i>Pseudonereis variegata</i> (Grube, 1857)	KC840693	KC833493	HQ705183

(Medlin *et al.* 1988) and 18SB 5'-ACCTTGTTACGACTTTTACTTCCTC-3' (Nygren & Sundberg 2003). Around 450 bp of 16S rRNA (16S) were amplified using the primers ann16Sf 5'-GCGGTATCCTGACCGTRCWAAGGTA-3' (Sjölin *et al.* 2005) and 16SbrH 5'-CCGGTCTGAACTCAGATCACGT-3' (Palumbi 1996), and around 650 bp of cytochrome *c* oxidase subunit I (COI) were amplified using LCO1490 5'-GGTCAACAAATCATAAAGATATTGG-3' (Folmer *et al.* 1994) and COI-E 5'-TATACTTCTGGGTGTCCGAAGAATCA-3' (Bely & Wray 2004). PCR mixtures contained 1 µl of each primer (10 µM), 2 µl template DNA and 21 µl of Red Taq DNA Polymerase 1.1X MasterMix (VWR) in a total mixture of 25 µl. The PCR amplification profile consisted of initial denaturation at 95°C for 5 min, 35 cycles of denaturation at 94°C for 45 s, annealing at 55°C for 45 s, extension at 72°C for 2 min and a final extension at 72°C for 10 min. PCR products were purified using the Millipore Multiscreen 96-well PCR Purification System and sequencing was performed on an ABI 3730XL DNA Analyser (Applied Biosystems) at the Natural History Museum Sequencing Facility, using the same primers as in the PCR reactions plus two internal primers for 18S, 620F 5'-TAAAGYTGYTGCAGTTAAA-3' (Nygren & Sundberg 2003) and 1324R 5'-CGGCCATGCACCACC-3' (Cohen *et al.* 1998). Overlapping sequence fragments were merged into consensus sequences using Geneious (Kearse *et al.* 2012). The sequences obtained in this study were aligned together with sequences from Genbank (Table 1) using MAFFT (Katoh 2002) for 18S and 16S, and MUSCLE (Edgar 2004) for COI, both programs used as plugins in Geneious, with default settings. The 18S alignment consisted of 1819 characters, 16S of 514 characters and the COI alignment of 657 characters.

In total 47 terminal taxa were used in the phylogenetic analyses, with 44 from Nereididae, and three taxa from Hesionidae Grube, 1850, another family within Nereidiformia, as the outgroup. While some earlier studies suggest that Chrysopetalidae Ehlers, 1864 is sister taxon to Nereididae (Dahlgren *et al.* 2000), later analyses have indicated that the Nereidiformia relationships are unresolved (Weigert & Bleidorn 2016), which justify the use of Hesionidae as the outgroup here. The program jModelTest (Posada 2008) was used to assess the best model for each partition (18S, 16S and COI) with BIC, which suggested GTR+I+G as the best model for all genes. The data was partitioned into the three parts (18S, 16S and COI) and this evolutionary model was applied to each partition. The parameters used for the partitions were unlinked. Bayesian phylogenetic analyses (BAs) were conducted with MrBayes ver. 3.2.6 (Ronquist *et al.* 2012). Analyses were run three times for 10 000 000 generations. Of these, the first 2 500 000 generations were discarded as burn-in. Tree files were interpreted with FigTree ver. 1.4.2 (available from <http://tree.bio.ed.ac.uk/software/figtree/>).

Data management

The management and transfer of specimen data between a central museum database, a molecular collections database, and external data repositories and aggregators (e.g., GenBank, World Register of Marine Species (WoRMS), Ocean Biodiversity Information System (OBIS), Global Biodiversity Information Facility (GBIF), Global Genome Biodiversity Network (GGBN), and ZooBank) was carried out through the usage of DarwinCore data standards (Wieczorek *et al.* 2012) including the GGBN DarwinCore extensions (Droege *et al.* 2016). See Glover *et al.* (2016) for further elaboration of this data pipeline. All specimens and DNA vouchers are archived in the Natural History Museum London collections. All specimen occurrence (and associated preparation) data are provided in a DarwinCore Archive (DWcA) in the supplementary material (Supp. file 1). All mapping was carried out using ArcGIS ver. 10.2.2.

Institutional abbreviations

NHMUK = Natural History Museum, London, UK
ZMH = Zoological Museum Hamburg

Results

Phylum Annelida Lamarck, 1809
Class Polychaeta Grube, 1850
Order Phyllodocida Dales, 1962
Family Nereididae Blainville, 1818

Neanthes Kinberg, 1865

Neanthes Kinberg, 1865: 171.

Neanthes – Fauchald 1977: 89. — Wilson 1984: 210; 1988: 5. — Wu *et al.* 1985: 143–144. — Bakken & Wilson 2005: 527. — Glasby *et al.* 2011: 363. — Sato 2013: 35. — Ibrahim *et al.* 2019: 85.

Type species

Neanthes vaalii Kinberg, 1865 by subsequent designation (Hartman 1954: 27). Southern Australia.

Neanthes goodayi sp. nov.

urn:lsid:zoobank.org:act:C5CDA152-0C73-46BB-955F-9BD5F02BE0F6

Figs 2–6, 8

Diagnosis

Anterior eye pair very large, distinct, posterior eyes minute. Postero-dorsal tentacular cirri reaching chaetigers 8–12. Two pigmented spots on dorsum of apodous segment. Palpostyles and palpophores rounded, spherical to ovoid. Paragnaths in pharyngeal areas: I = 1–2, II = 9–12, III = 6, IV = 12–16, V = 0, VI = 1–4, VII–VIII = 12–19; area VI–I–VI pattern λ-shaped on oral ring. Chaetigers 1–2 uniramous, remaining chaetigers biramous. Parapodial lobes conical, becoming narrower in posterior chaetigers. Neuracicular postchaetal lobe longer than or equal to neuracicular ligule on anterior chaetigers, shorter on medial chaetigers, papilliform or absent on posterior chaetigers. Dorsal cirri exceed length of ligules on anterior chaetigers, as long as or slightly shorter than ligules on medial chaetigers, becoming longer and exceeding ligules towards posterior end; on largest specimens, dorsal cirri exceed ligules on all chaetigers. Notochaetae with homogomph spinigers throughout, supracicular neurochaetae with homogomph spinigers and heterogomph falcigers throughout, subacicular neurochaetae with homogomph spinigers, homogomph falcigers and heterogomph falcigers throughout.

Etymology

Named in honor of Andy Gooday, member of the science party of both ABYSSLINE cruises. This etymology is part of the ABYSSLINE naming convention where all new taxon names are based on a randomised list of both crew and scientists of the two research cruises in order to recognise the team effort involved in this extensive sampling program (Wiklund *et al.* 2019).

Material examined

Holotype

PACIFIC OCEAN • Eastern Central Pacific, Clarion Clipperton Fracture Zone; 12.53717° N, 116.60417° W; depth 4425 m; 20 Feb. 2015; A.G. Glover, H. Wiklund, T. Dahlgren and M. Brasier leg.; Brenke epibenthic sled, collected from epi-net; specimen guid: 21b3d59f-5ec4-40da-9d65-4177e7674f63, field ID: NHM_739, DNA voucher barcode: 0109493268, GenBank COI gene: MZ407918; NHMUK ANEA 2020.260.

Paratypes

PACIFIC OCEAN – **Eastern Central Pacific, Clarion Clipperton Fracture Zone** • 1 spec.; 13.75833° N, 116.69852° W; depth 4080 m; 11 Oct. 2013; A.G. Glover, H. Wiklund, T.G. Dahlgren and M.N. Georgieva leg.; Brenke epibenthic sled, collected from epi-net; specimen guid: 2d448c5f-bf70-4ed1-a541-9b505ec46434, field ID: NHM_127, DNA voucher barcode: 0109492959, GenBank 16S gene: MZ408645; NHMUK ANEA 2020.33 • 1 spec.; 13.93482° N, 116.55018° W; depth 4082 m; 14 Oct. 2013; same collectors and collection method as for preceding; specimen guid: f5f08fc7-49b4-446f-9f04-fbbca84f7886, field ID: NHM_171, DNA voucher barcode: 0109492952, GenBank 18S gene: MZ408643, 16S gene: MZ408646, COI gene: MZ407911; NHMUK ANEA 2020.34 • 1 spec.; 13.81167° N, 116.71° W; depth 4076 m; 16 Oct. 2013; same collectors as for preceding; USNEL box corer, collected from 0–2 cm fraction; specimen guid: fb66da6c-f627-487f-a386-3454541ad33a, field ID: NHM_238, DNA voucher barcode: 0109493276, GenBank 16S gene: MZ408648, COI gene: MZ407913; NHMUK ANEA 2020.36 • 1 spec.; 12.41628° N, 116.71485° W; depth 4127 m; 16 Feb. 2015; A.G. Glover, H. Wiklund, T.G. Dahlgren and M. Brasier leg.; USNEL box corer, collected from nodule; specimen guid: e1461d7d-c6c8-46fc-b951-f5ee88550a5b, field ID: NHM_512, DNA voucher barcode: 0109493273, GenBank 16S gene: MZ408651; NHMUK ANEA 2020.1 • 1 spec.; 12.53717° N, 116.60417° W; depth 4425 m; 20 Feb. 2015; same collectors as for preceding; Brenke epibenthic sled, collected from epi net; specimen guid: 0d2be1b6-4348-46a2-a1a7-b214562c7b18; field ID: NHM_790, DNA voucher barcode: 0109493261, GenBank 16S gene: MZ408660; NHMUK ANEA 2020.7 • 1 spec.; 12.25733° N, 117.30216° W; depth 4302 m; 1 Mar. 2015; same collectors and collection method as for preceding; specimen guid: bb93253e-2d66-4592-b569-cfa5976fed33, field ID: NHM_1254, DNA voucher barcode: 0109493252, GenBank 16S gene: MZ408667; NHMUK ANEA 2020.17 • 1 spec.; 12.59688° N, 116.49357° W; depth 4258 m; 9 Mar. 2015; same collectors as for preceding; USNEL box corer, collected from nodule; specimen guid: 333370c7-eb36-429c-96ed-fce5658f2ad2, field ID: NHM_1624, DNA voucher barcode: 0109493249, GenBank 16S gene: MZ408670; NHMUK ANEA 2020.20 • 1 spec.; 12.17383° N, 117.19283° W; depth 4045 m; 11 Mar. 2015; same collectors as for preceding; Brenke epibenthic sled, collected from epi-net; specimen guid: 6d7f58fc-a657-47f4-9261-7517228de6a1, field ID: NHM_1783, DNA voucher barcode: 0109493246, GenBank 16S gene: MZ408673, COI gene: MZ407927; NHMUK ANEA 2020.23 • 1 spec.; 12.02738° N, 117.3252° W; depth 4139 m; 17 Mar. 2015; same collectors as for preceding; USNEL box corer, collected from nodule; specimen guid: 8abc43ad-193d-4e35-b548-6d2d0b7777f8, field ID: NHM_2069, DNA voucher barcode: 0109493237, GenBank 16S gene: MZ408681; NHMUK ANEA 2020.31.

Other material

PACIFIC OCEAN – **Eastern Central Pacific, Clarion Clipperton Fracture Zone** • 1 spec.; 13.93482° N, 116.55018° W; depth 4082 m; 14 Oct. 2013; A.G. Glover, H. Wiklund, T.G. Dahlgren and M.N. Georgieva leg.; Brenke epibenthic sled, collected from epi-net; specimen guid: 022c1d2a-8b2a-479f-8ed2-20ff4e9610dd, field ID: NHM_173, DNA voucher barcode: 0109493277, GenBank 18S gene: MZ408644, 16S gene: MZ408647, COI gene: MZ407912; NHMUK ANEA 2020.35 • 1 spec.; 13.81167° N, 116.71° W; depth 4076 m; 16 Oct. 2013; same collectors as for preceding; USNEL box corer, collected from 0–2 cm fraction; specimen guid: 57002bc8-fa3a-4a55-b823-0af978cd2fed, field ID: NHM_239, DNA voucher barcode: 0109493275, GenBank 16S gene: MZ408649, COI gene: MZ407914; NHMUK ANEA 2020.37 • 1 spec.; same collection data as for preceding; specimen guid: 4a8718c5-d675-4044-9d2b-613fld8d5fda, field ID: NHM_240, DNA voucher barcode: 0109493274, GenBank 16S gene: MZ408650, COI gene: MZ407915; NHMUK ANEA 2020.38 • 1 spec.; 12.38624° N, 116.54867° W; depth 4202 m; 17 Feb. 2015; A.G. Glover, H. Wiklund, T.G. Dahlgren and M. Brasier leg.; Brenke epibenthic sled, collected from epi-net; specimen guid: f61f9136-a39a-4696-8fdc-68aee0af5101, field ID: NHM_614, DNA voucher barcode: 0109493272, GenBank 16S gene: MZ408652, COI gene: MZ407916; NHMUK ANEA 2020.2 • 1 spec.; same collection data as for preceding; specimen guid: 1033aa6b-4093-41fc-af75-9ad090dd4c56, field

ID: NHM_644, DNA voucher barcode: 0109493271, GenBank 16S gene: MZ408653, COI gene: MZ407917; NHMUK ANEA 2020.257 • 1 spec.; 12.53717° N, 116.60417° W; depth 4425 m; 20 Feb. 2015; same collectors and collection method as for preceding; specimen guid: 9a97230a-4b78-4823-88a5-d02d9c874db9; field ID: NHM_678, DNA voucher barcode: 0109493270, GenBank 16S gene: MZ408654; NHMUK ANEA 2020.258 • 1 spec.; same collection data as for preceding; specimen guid: 954c9c61-3e45-45a4-8522-7aadd1c86c60; field ID: NHM_692, DNA voucher barcode: 0109493269, GenBank 16S gene: MZ408655; NHMUK ANEA 2020.259 • 1 spec.; same collection data as for preceding; specimen guid: 76f62614-0cae-4177-8312-e231f5107f8c; field ID: NHM_743, DNA voucher barcode: 0109492976, GenBank 16S gene: MZ408656; NHMUK ANEA 2020.261 • 1 spec.; same collection data as for preceding; specimen guid: 3951d751-f1ba-44ae-8368-261047c07b12; field ID: NHM_755, DNA voucher barcode: 0109493257, GenBank COI gene: MZ407919; NHMUK ANEA 2020.3 • 1 spec.; same collection data as for preceding; specimen guid: 67a9133b-c57b-49c6-b6e4-124eb1315eac; field ID: NHM_757, DNA voucher barcode: 0109493258, GenBank 16S gene: MZ408657; NHMUK ANEA 2020.4 • 1 spec.; same collection data as for preceding; specimen guid: b13dc262-c631-44dc-927e-6a04c3608bda; field ID: NHM_766, DNA voucher barcode: 0109493259, GenBank 16S gene: MZ408658; NHMUK ANEA 2020.5 • 1 spec.; same collection data as for preceding; specimen guid: d9e557c5-3ffd-4a39-9eed-5eceed5e735f; field ID: NHM_783A, DNA voucher barcode: 0109493260, GenBank 16S gene: MZ408659; NHMUK ANEA 2020.6 • 1 spec.; same collection data as for preceding; specimen guid: 792a4c9a-9653-4ce1-8683-ca2556c1999a8; field ID: NHM_793, DNA voucher barcode: 0109493262, GenBank COI gene: MZ407920; NHMUK ANEA 2020.8 • 1 spec.; 12.57903° N, 116.68697° W; depth 4237 m; 22 Feb. 2015; same collectors as for preceding; USNEL box corer, collected from 0–2 cm fraction; specimen guid: a933dd63-64d1-4e45-95ad-7d68282dd892; field ID: NHM_865, DNA voucher barcode: 0109493263, GenBank COI gene: MZ407921; NHMUK ANEA 2020.9 • 1 spec.; 12.57133° N, 116.6105° W; depth 4198 m; 23 Feb. 2015; same collectors as for preceding; Brenke epibenthic sled, collected from epi-net; specimen guid: 3e7262c7-fd75-4a53-9d6c-9d01955d1bef; field ID: NHM_950, DNA voucher barcode: 0109493264, GenBank 16S gene: MZ408661, COI gene: MZ407922; NHMUK ANEA 2020.10 • 1 spec.; same collection data as for preceding; specimen guid: 06c15319-2b89-4899-b2e5-1fcd8e4a9413; field ID: NHM_971, DNA voucher barcode: 0109493265, GenBank COI gene: MZ407923; NHMUK ANEA 2020.11 • 1 spec.; 12.13367° N, 117.292° W; depth 4122 m; 24 Feb. 2015; same collectors and collection method as for preceding; specimen guid: 165a459f-8b81-4e97-8e82-cdcd013e1ed1; field ID: NHM_1011, DNA voucher barcode: 0109493266, GenBank 16S gene: MZ408662, COI gene: MZ407924; NHMUK ANEA 2020.12 • 1 spec.; 12.1155° N, 117.1645° W; depth 4100 m; 26 Feb. 2015; same collectors and collection method as for preceding; specimen guid: a343e242-410a-4817-98c6-7125db7d03e7; field ID: NHM_1079, DNA voucher barcode: 0109493267, GenBank 16S gene: MZ408663; NHMUK ANEA 2020.13 • 1 spec.; same collection data as for preceding; specimen guid: 7ead0546-d0bd-4381-83af-89f58d8f8f4c; field ID: NHM_1167A, DNA voucher barcode: 0109492975, GenBank 16S gene: MZ408664; NHMUK ANEA 2020.14 • 1 spec.; same collection data as for preceding; specimen guid: 6b51d602-83f1-4bb4-b71a-e85cdbcb8e8dc; field ID: NHM_1171, DNA voucher barcode: 0109493254, GenBank 16S gene: MZ408665, COI gene: MZ407925; NHMUK ANEA 2020.15 • 1 spec.; 12.00945° N, 117.17812° W; depth 4144 m; 27 Feb. 2015; same collectors as for preceding; USNEL box corer, collected from nodule; specimen guid: 9e903864-55e8-4a1a-b532-c47af39b95f4; field ID: NHM_1194, DNA voucher barcode: 0109493253, GenBank 16S gene: MZ408666; NHMUK ANEA 2020.16 • 1 spec.; 12.45433° N, 116.61283° W; depth 4137 m; 3 Mar. 2015; same collectors as for preceding; Brenke epibenthic sled, collected from epi-net; specimen guid: e5797775-7141-4eb5-bb5e-dbcdb29f7b42e; field ID: NHM_1480E, DNA voucher barcode: 0109493251, GenBank 16S gene: MZ408668; NHMUK ANEA 2020.18 • 1 spec.; 12.51317° N, 116.49133° W; depth 4252 m; 5 Mar. 2015; same collectors and collection method as for preceding; specimen guid: 35bae0ad-f00e-442b-a8f5-b1b318bf1015; field ID: NHM_1515, DNA voucher barcode: 0109493250,

GenBank 16S gene: MZ408669, COI gene: MZ407926; NHMUK ANEA 2020.19 • 1 spec.; 12.59688° N, 116.49357° W; depth 4258 m; 9 Mar. 2015; same collectors as for preceding; USNEL box corer, collected from nodule; specimen guid: 29f1c1bf-5bca-4ed1-a893-edcd45493e04; field ID: NHM_1631A, DNA voucher barcode: 0109493248, GenBank 16S gene: MZ408671; NHMUK ANEA 2020.21 • 1 spec.; 12.17383° N, 117.19283° W; depth 4045 m; 11 Mar. 2015; same collectors as for preceding; Brenke epibenthic sled, collected from epi-net; specimen guid: 83507a57-c168-4b6f-b984-1c69ccbcbec27; field ID: NHM_1764, DNA voucher barcode: 0109493247, GenBank 16S gene: MZ408672; NHMUK ANEA 2020.22 • 1 spec.; 12.0999° N, 117.1966° W; depth 4051 m; 12 Mar. 2015; same collectors as for preceding; USNEL box corer, collected from 0–2 cm fraction; specimen guid: f79fb7b6-ed29-4cc3-9f7f-8d4ace75c585; field ID: NHM_1836A, DNA voucher barcode: 0109493245, GenBank 16S gene: MZ408674; NHMUK ANEA 2020.24 • 1 spec.; 12.0415° N, 117.21717° W; depth 4094 m; 13 Mar. 2015; same collectors as for preceding; Brenke epibenthic sled, collected from epi-net; specimen guid: 0508d326-ef73-4f52-bdc6-757b2ab745fe; field ID: NHM_1866, DNA voucher barcode: 0109492983, GenBank 16S gene: MZ408675, COI gene: MZ407928; NHMUK ANEA 2020.25 • 1 spec.; same collection data as for preceding; specimen guid: 922ad1d7-bd75-4588-ba2e-be32cfe432c5; field ID: NHM_1891, DNA voucher barcode: 0109492960, GenBank 16S gene: MZ408676; NHMUK ANEA 2020.26 • 1 spec.; same collection data as for preceding; specimen guid: e991eafe-0593-4e08-8967-d77e017eabac; field ID: NHM_1929A, DNA voucher barcode: 0109493233, GenBank 16S gene: MZ408677, COI gene: MZ407929; NHMUK ANEA 2020.27 • 1 spec.; same collection data as for preceding; specimen guid: 62b28de1-a797-4ec0-99cf-e38625b0e01c; field ID: NHM_1929B, DNA voucher barcode: 0109493234, GenBank 16S gene: MZ408678; NHMUK ANEA 2020.28 • 1 spec.; same collection data as for preceding; specimen guid: 25953aef-8a48-48d1-9fc2-b0a86ec7d052; field ID: NHM_1947D, DNA voucher barcode: 0109493235, GenBank 16S gene: MZ408679; NHMUK ANEA 2020.29 • 1 spec.; 12.0505° N, 117.40467° W; depth 4235 m; 16 Mar. 2015; same collectors and collection method as for preceding; specimen guid: d8edb41d-51d6-4fbd-a547-92fa290209d4; field ID: NHM_2014, DNA voucher barcode: 0109493236, GenBank 16S gene: MZ408680, COI gene: MZ407930; NHMUK ANEA 2020.30 • 1 spec.; 12.57133° N, 116.6105° W; depth 4198 m; 23 Feb. 2015; same collectors as for preceding; Brenke epibenthic sled, collected from supra-net; specimen guid: 1c30624d-19a0-43f0-92dc-9a315a3e43fc; field ID: NHM_3074, DNA voucher barcode: 0109493238, GenBank 16S gene: MZ408682; NHMUK ANEA 2020.32.

Comparative material examined

Holotype of *Neanthes heterocolata* (Hartmann-Schröder, 1981)

ATLANTIC OCEAN • Northeastern Atlantic, Bay of Biscay; 46°35.0' N, 7°45.5' W; depth 4700 m; 24 Oct. 1967; ZMH P-16464.

Paratypes of *Neanthes heterocolata* (Hartmann-Schröder, 1981)

ATLANTIC OCEAN • 2 specs; same collection data as for preceding; ZMH P-16465.

Description

Holotype (NHM_739) complete, TL = 12 mm, L15 = 4.7 mm, W15 = 0.9 mm, for 47 chaetigers. Body somewhat 'baseball bat-shaped', wide, swollen anteriorly but tapering gradually posteriorly (Fig. 2A–B). Live specimen pale, iridescent and semi-translucent, with yellow gut and red blood vessels visible through body wall (Fig. 2A, C); specimen in ethanol opaque, pale beige, with some red vasculature still visible (Fig. 2B, D). Two pigmented spots on either side of dorsum of apodous segment visible in both live specimens and in ethanol, with some pigmentation also visible on dorsum of anterodorsal tentacular cirrophores (Fig. 2C–D).

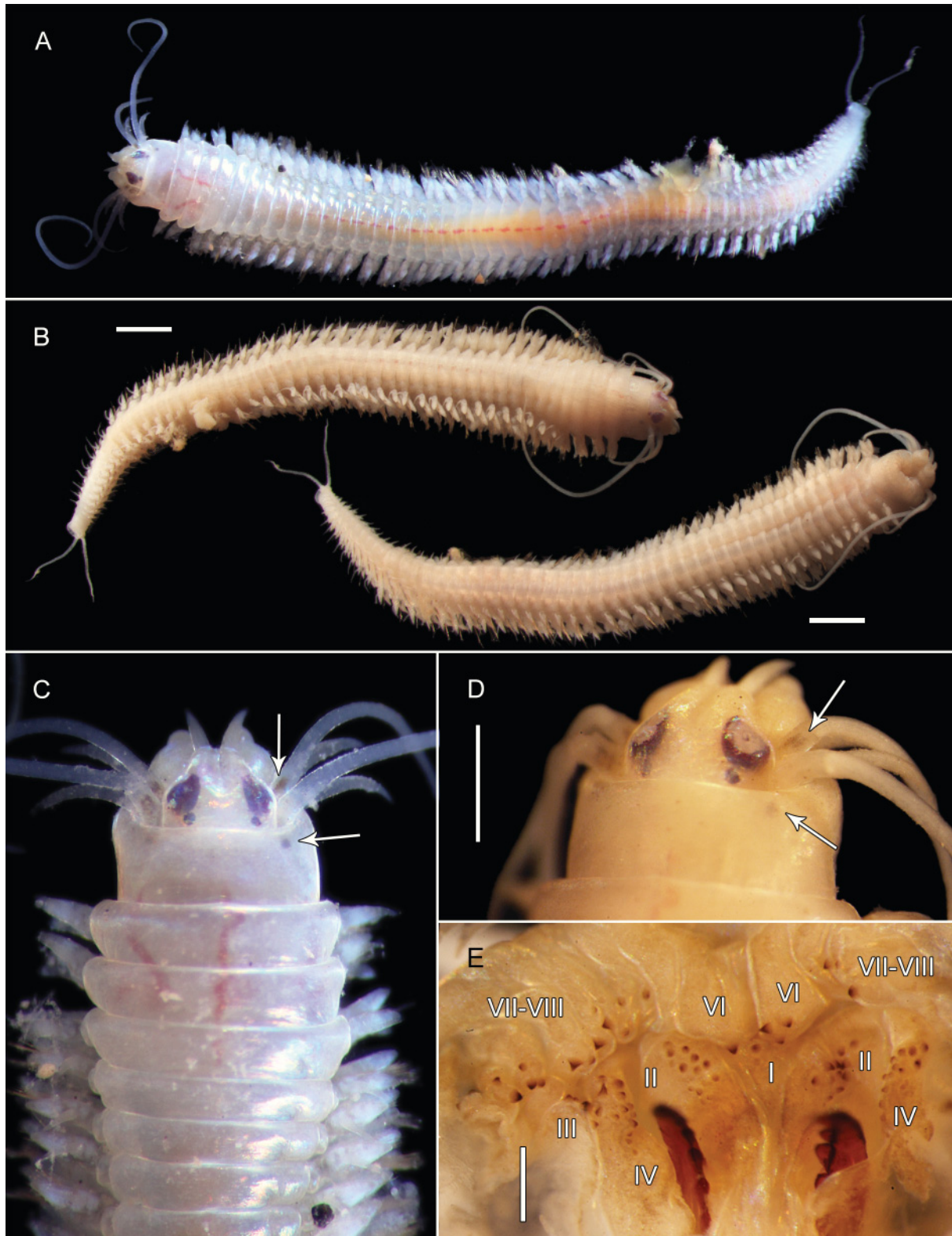


Fig. 2. *Neanthes goodayi* sp. nov., holotype (NHM_739). **A.** Live image, entire specimen. **B.** Preserved entire specimen, dorsal view (left), ventral view (right). **C.** Live image, anterior view, arrows mark pigmentation. **D.** Preserved specimen, anterior view, arrows mark pigmentation. **E.** Dissected pharynx, with pharyngeal areas I, II, III, IV, VI, VII–VIII highlighted. Scale bars: B = 1 mm; D = 500 μ m; E = 250 μ m.

Prostomium short, rounded trapezoid with shallow dorsal depression extending anteriorly from midpoint to distal margin (Fig. 2C–D); antennae cirriform, medium-sized, barely extending beyond palps. Palps nearly as long as prostomium, with both palpophores and palpostyles short, spherical, with palpostyles half as long as palpophores. Tentacular cirri with short, cylindrical cirrophores; posterior-dorsal pair of tentacular cirri longest, extending to chaetiger 12 (Fig. 2A–B). Two pairs of dark red eyes; anterior pair very large, rounded teardrop-shaped, with large, rounded lenses inserted anterolaterally and with an iris-like structure visible in preserved specimen (Fig. 2C); posterior pair of eyes minute, rounded, with small anterolateral lenses. Apodous anterior segment collar-like, slightly longer and narrower than chaetiger 1.

Pharynx not everted. Jaws dark red-brown with 6 lateral teeth; All paragnaths brown, conical, arranged as follows (Fig. 2E): area I: 2, one large cone, one smaller cone distally; area II: 12 in cluster; area III: approx. 6 (area damaged), four cones in row with two smaller cones laterally; area IV: 13 in teardrop-shaped cluster, with curved line of cones extending from jaws posteriorly, ending in cluster of 7 cones; area V: no paragnaths; area VIa: 1; area VIb: 4, one large and three smaller cones in trapezoid arrangement; areas VII–VIII: 19, eight large cones in a single well-spaced row with 11 smaller cones scattered laterally. Areas VI–V–VI with λ -shaped ridge pattern.

Chaetigers 1 and 2 uniramous, with all subsequent chaetigers biramous.

Dorsal cirri inserted at base of median and dorsal ligule in uniramous and biramous chaetigers, respectively, slightly inflated on uniramous chaetigers (Fig. 3A), more slender from chaetiger 3 onwards (Fig. 3B–H); dorsal cirri extending beyond median ligule on anteriormost chaetigers (Fig. 3A–B), as long as or slightly shorter than median ligules from chaetiger 6 onwards (Fig. 3C–D) and extending beyond median ligules from around chaetiger 29 (Fig. 3E), up to twice as long as median ligules on posterior chaetigers from chaetiger 40 (Fig. 3G–H).

Dorsal ligule conical throughout, slightly shorter than median ligules on anterior chaetigers (Fig. 3B–C), approximately two-thirds the length of median ligules from chaetiger 10 onwards. Dorsal and median ligules reduced in size on posterior chaetigers from chaetiger 40, with dorsal ligule vanishing in posteriormost chaetigers (Fig. 3H). Median ligule slightly inflated on uniramous chaetigers (Fig. 3A), conical on biramous chaetigers, narrower from chaetiger 29 (Fig. 3E), bluntly conical on posteriormost chaetigers (Fig. 3H). Notopodial prechaetal lobe indistinct.

Neuracicular ligule shorter than ventral neuropodial ligule on anterior chaetigers (Fig. 3A–C), becoming equal in length or slightly shorter from chaetiger 10, equal or slightly longer from chaetiger 29 (Fig. 3E). Superior neuropodial lobe indistinct, truncate throughout; inferior lobe short, rounded on anterior and medial chaetigers, gradually shortening, giving neuracicular ligule pointed appearance on posterior chaetigers (Fig. 3G–H). Neuracicular prechaetal lobe indistinct. Neuracicular postchaetal lobe conical, longer than neuracicular lobe on anteriormost chaetigers (Fig. 3A–B), equal in length at chaetiger 6 (Fig. 3C), gradually shortening and becoming more digitiform on subsequent chaetigers to papilliform nub around chaetiger 29 (Fig. 3F), absent in posterior chaetigers from around chaetiger 40.

Ventral neuropodial ligule conical throughout, gradually narrowing on medial (Fig. 3E) and posterior chaetigers (Fig. 3G–H). Ligule sub-equal in length to median ligule in anterior and early medial chaetigers (Fig. 3A–D), becoming shorter in remaining chaetigers from chaetiger 29 (Fig. 3E), to two-thirds as long as ligule from chaetiger 40 (Fig. 3G) and half as long on posteriormost chaetigers (Fig. 3H).

Ventral cirri cirriform (Fig. 3C–F), inserted basally to ventral neuropodial ligule throughout, slightly shorter than ligule on anterior and medial chaetigers, subequal in length on posteriormost chaetigers (Fig. 3F).

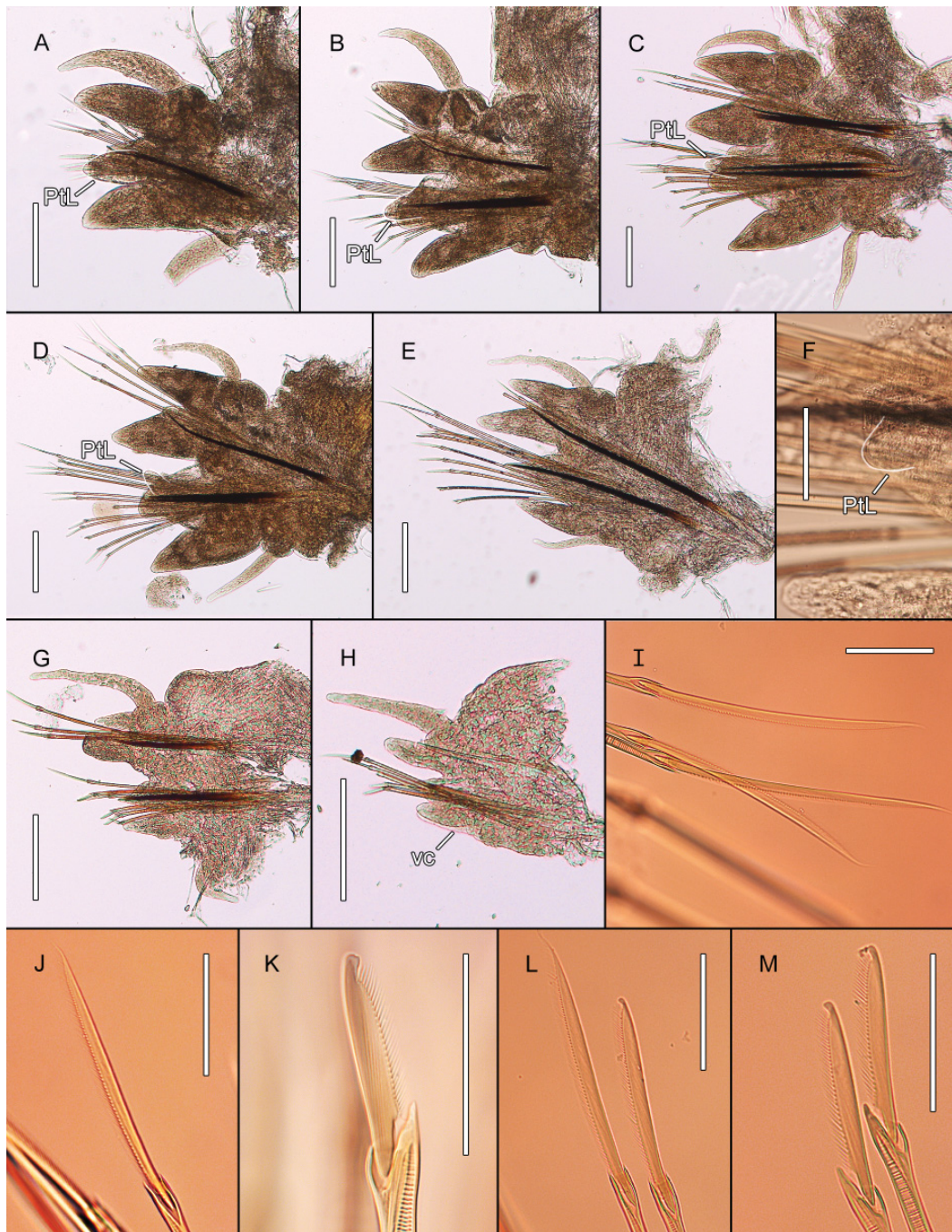


Fig. 3. *Neanthes goodayi* sp. nov., holotype (NHM_739). **A.** Chaetiger 1, posterior view. **B.** Chaetiger 3, posterior view. **C.** Chaetiger 6, posterior view. **D.** Chaetiger 20, posterior view. **E.** Chaetiger 29, posterior view. **F.** Chaetiger 29, posterior view, detail of neuracicular postchaetal lobe. **G.** Chaetiger 40, posterior view. **H.** Chaetiger 46, posterior view. **I.** Notochaetae, detail of homogomph spinigers, chaetiger 20. **J.** Supracicular neurochaetae, detail of homogomph spiniger, chaetiger 3. **K.** Supracicular neurochaetae, detail of heterogomph falciger, chaetiger 10. **L.** Subacicular neurochaetae, detail of homogomph spiniger (left) and homogomph falciger (right), chaetiger 20. **M.** Subacicular neurochaetae, detail of heterogomph falcigers, chaetiger 20. Abbreviations: PtL = postchaetal lobe; VC = ventral cirrus. Postchaetal lobe in A–D, F outlined with a fine white line. Parapodia in C, E–H dissected from left side of specimen; parapodia in A–B, D dissected from right side of specimen, with images laterally inverted follow direction of other plates. Scale bars: A–E, G–H = 200 μ m; F, I–M = 50 μ m.

Pygidium somewhat pyriform, truncate distally, with two filamentous anal cirri attached ventro-laterally, extending 8 chaetigers in length (Fig. 2A–B).

Caecal glands present, small, white, slightly thickened.

Multiple aciculae per parapodial lobe observed on some chaetigers in holotype: double neuracaculae in chaetigers 2, 3, 6 and 20 (Fig. 3B–D), and triple notoacaculae on chaetiger 6 (Fig. 3C). This feature was not observed in parapodial dissections from paratypes.

Notochaetae all homogomph spinigers with long blades, of similar width towards toothed edge but drastically slendering to an aristate distal end (Fig. 3I); 4 present in anterior chaetigers, 5 in medial chaetigers, 3 in posterior chaetigers and absent from chaetiger 46.

Supracicular neurochaetae with homogomph spinigers and heterogomph falcigers, both types present in all falcigers except final two chaetigers, where supracicular falcigers are absent. Homogomph spinigers similar in appearance to those of notopodia (Fig. 3J), though with blades reducing in length moving ventrally (shortest blades two-thirds as long as longest blade), numbering 4 on first two chaetigers, 3–5 on anterior and medial chaetigers and 2 on posterior chaetigers where fascicles remain. Heterogomph falcigers with knob-like tips (Fig. 3K) and blades roughly half the length of shortest spinigers, numbering 1 on anterior chaetigers, 2 on medial chaetigers and 1 on posterior chaetigers where fascicles remain.

Subacicular neurochaetae with homogomph spinigers and both homogomph and heterogomph falcigers. Homogomph spinigers also similar in appearance to those of notopodia (Fig. 3L) but with blades two-thirds as long and numbering 1–2 on all chaetigers. Homogomph falcigers with knob-like tips (Fig. 3L), blades three-quarters the length of spinigers (Fig. 3L), numbering 1–3 on all chaetigers. Heterogomph falcigers similar in appearance to those of supracicular fascicles (Fig. 3M), numbering 3 on first two chaetigers, 4–6 on anterior, 2–4 on medial and 2–3 on posterior chaetigers.

Variations

Largest specimen (paratype NHM_2069) damaged, in two parts, TL = 17 mm, L15 = 6.7 mm, W15 = 1 mm for 55 chaetigers. Smallest specimen (paratype NHM_127) with TL = 1 mm for 10 chaetigers (see Juveniles section below). Pigment spots on dorsum as in holotype, consistent across most specimens both live and preserved (Fig. 4A–D), pigmentation on tentacular cirrophores more variable. Palpophores spherical to ovoid in shape (e.g., Fig. 4B). Posterior-dorsal pair of tentacular cirri extending to chaetiger 8–12 in most specimens (max. chaetiger 6 in juveniles). Eyes dark red to purple, anterior pair ranging from circular/ovoid (Fig. 4B–D) to teardrop-shaped concave discs or deeper cups (Figs 4A, 5A), becoming more crescent-shaped with decreasing size (Fig. 5B–D); posterior pair mostly circular (Fig. 4A–B), but occasionally oblong (Fig. 4A) or seeming to fuse with anterior pair (Fig. 6A–B), or with one missing (Fig. 4D). Posterior eye pair often less distinct in smaller specimens (Fig. 5A–B), becoming tiny spots (Fig. 5A) or patchy and irregularly shaped (Fig. 5B), completely absent in smallest specimens (Fig. 5C–D), with trace of lens not obvious. Apodous anterior segment longer and narrower than chaetiger 1, as in holotype, to similar in length and width as chaetiger 1 (Fig. 4A–D).

Jaws with 6–7 lateral teeth; paragnaths in pharangeal areas in non-holotype specimens: I = 1–2, II = 9–12, III = 6, IV = 12–16, V = 0, VI = 2–3, VII–VIII = 12–17 (8 large cones in a row as in holotype, varying number of smaller cones scattered laterally). Only one specimen (epitoke male, paratype NHM_1783) with pharynx everted (Fig. 6B).

In largest specimen, dorsal cirrus exceeds median ligule on all chaetigers, neuracicular ligule remains slightly longer than ventral ligule on median and posterior chaetigers, prechaetal lobe remains as

visible papilliform process on posterior chaetigers, ventral ligule subequal to ventral ligule from medial chaetigers onwards and ventral cirri longer than ventral ligule on posteriormost chaetigers.

Numbers of chaetae greater for most fascicles in largest specimen: notochaetae 6 homogomph spinigers on anterior and medial chaetigers, 4 in posterior chaetigers, 1 in posteriormost chaetigers; supracicular neurochaetae with 5–7 homogomph spinigers on first two chaetigers, 2–4 on anterior and medial chaetigers, 1 on posterior chaetigers, heterogomph falcigers 3 on first two chaetigers, 4–6 on anterior chaetigers, 0–3 on medial chaetigers and 1 on posterior chaetigers; subacicular neurochaetae with 2–4 homogomph spinigers most chaetigers, 1 on posteriormost chaetigers, homogomph falcigers 3–5 on

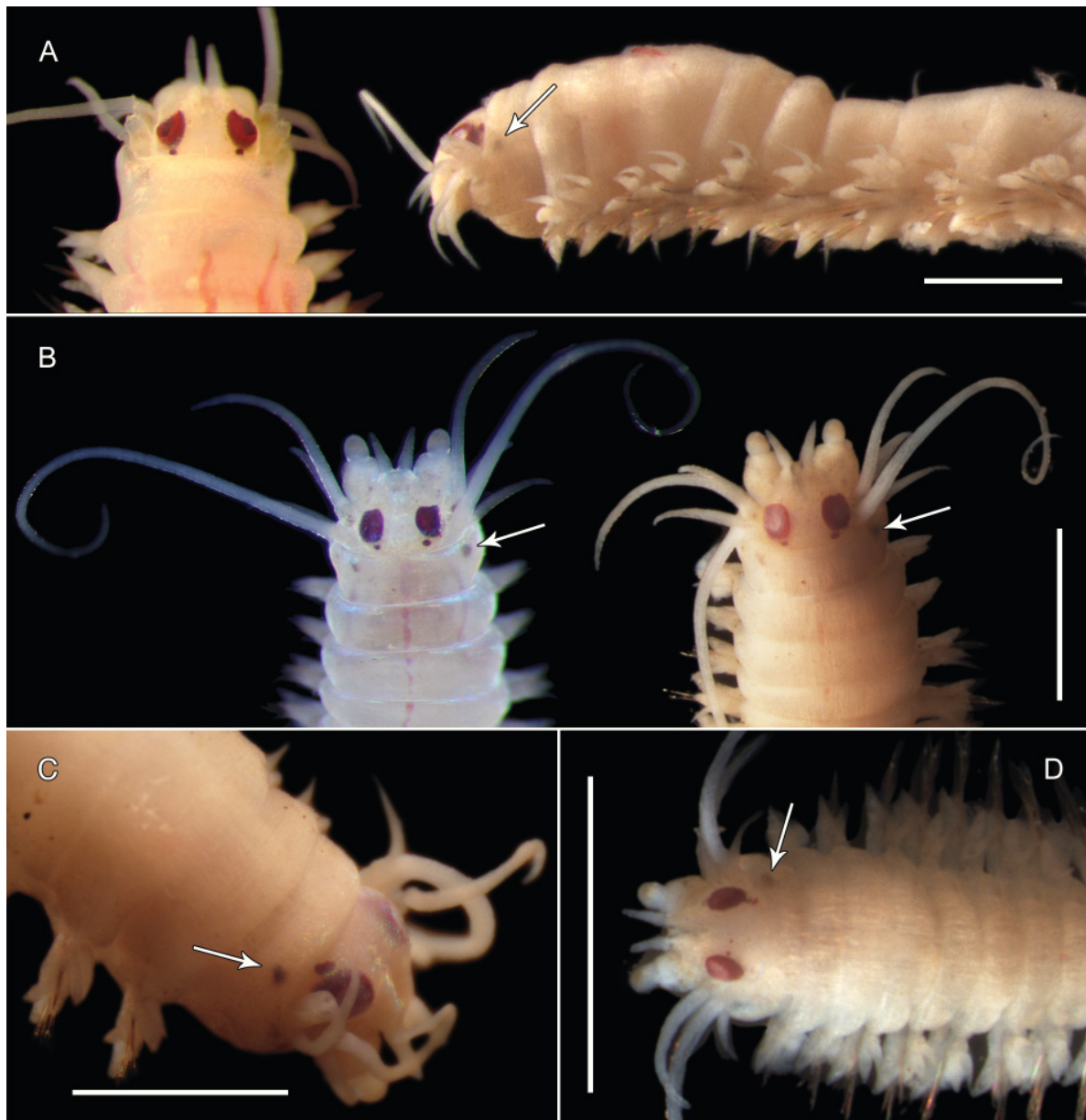


Fig. 4. *Neanthes goodayi* sp. nov., paratypes. **A.** Paratype (NHM_1624), preserved specimen; dorsal anterior view, live image (left); lateral anterior view, preserved specimen (right). **B.** Paratype (NHM_755); dorsal anterior view, live image (left), preserved specimen (right); arrows marking pigmentation. **C.** Paratype (NHM_238), dorsal anterior view, arrows mark pigmentation. **D.** Paratype (NHM_512), dorsal anterior view, arrows mark pigmentation. Scale bars = 1 mm.

anterior chaetigers, 1–2 on medial chaetigers, 1 on posterior chaetigers, heterogomph falcigers 6–9 on anterior chaetigers, 1–3 on medial and posterior chaetigers.

Description of epitoke paratype

One epitokous specimen observed (paratype NHM_1783) (Fig. 6A). Specimen moderately damaged, posteriorly incomplete, TL= 10 mm, L15 = 4 mm, for 37 chaetigers (chaetiger 15 damaged, width at chaetiger 14 excluding parapodia 0.8 mm). Body divided into two regions: pre-natatory with 14 chaetigers and natatory with at least 23 chaetigers; post-natatory region unknown. Eyes not notably modified (Fig. 6A–B); anterior pair with iris-like structure as in holotype, posterior pair somewhat fused to anterior pair.

Pre-natatory chaetigers with modified dorsal and ventral cirri on chaetigers 1–7; notably thickened, but with distalmost tip remaining fine and cirriform (Fig. 6C). Chaetal types in pre-natatory chaetigers as in holotype.

Natatory chaetigers with distinctly enlarged, elongate modified parapodia (Fig. 6D). Noto- and neuropodia elongated basally, with ligules and lobes not significantly larger than on non-modified parapodia. Neuracicular ligule with lamellar structure distally. Both dorsal and ventral cirri notably elongate, with a pair of conical lobes emerging from the upper and lower base of each cirrus, not present on anterior chaetigers; dorsal cirri slightly papillated (Fig. 6D–E). Both notopodial and neuropodial fascicles dense, up to 40 chaetae per fascicle, and with only a single chaetal type: long, simple sesquigomph spinigers

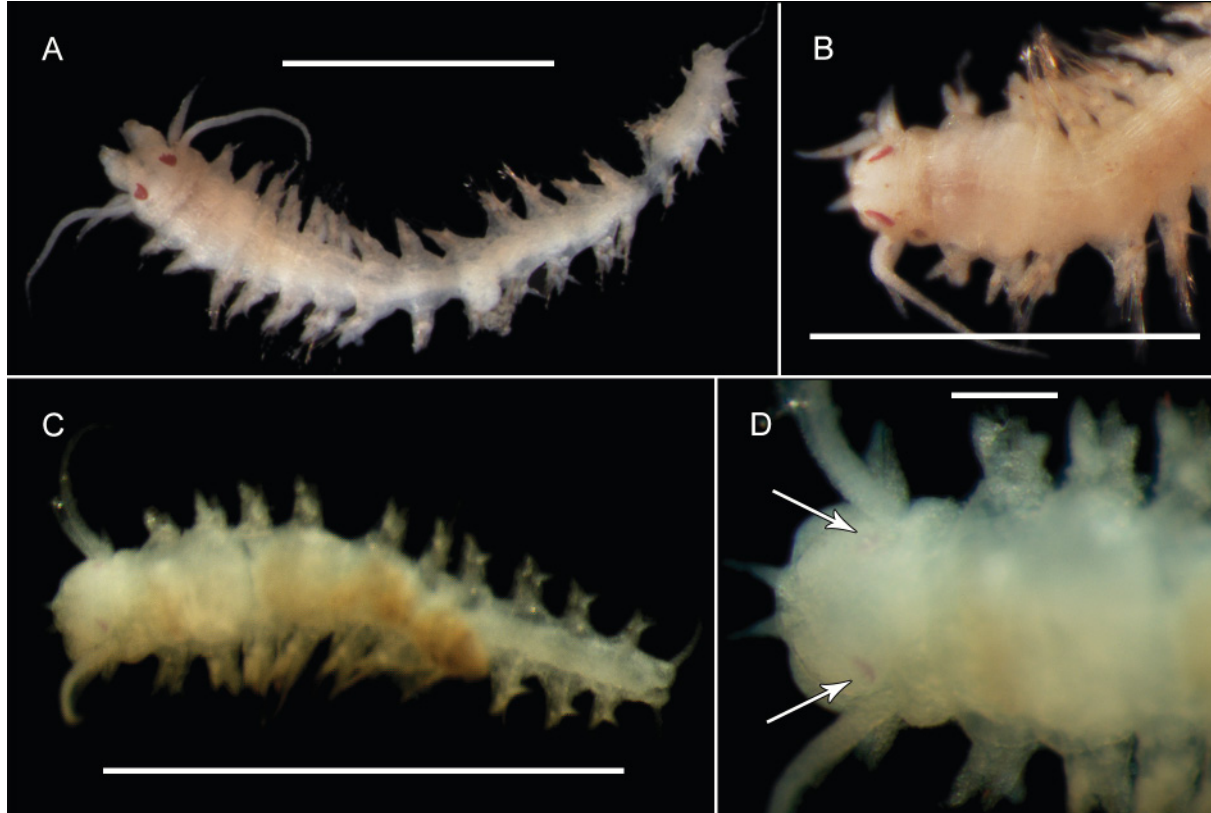


Fig. 5. *Neanthes goodayi* sp. nov., juvenile specimens. **A.** Paratype (1254), entire specimen, dorsal view. **B.** Paratype (NHM_171) dorsal anterior view. **C.** Paratype (NHM_127) entire specimen, dorsal view. **D.** Paratype (NHM_127), close up of dorsal anterior, arrows mark position of anterior eye pair. Scale bars: A, C = 1 mm; B = 500 µm; D = 100 µm.

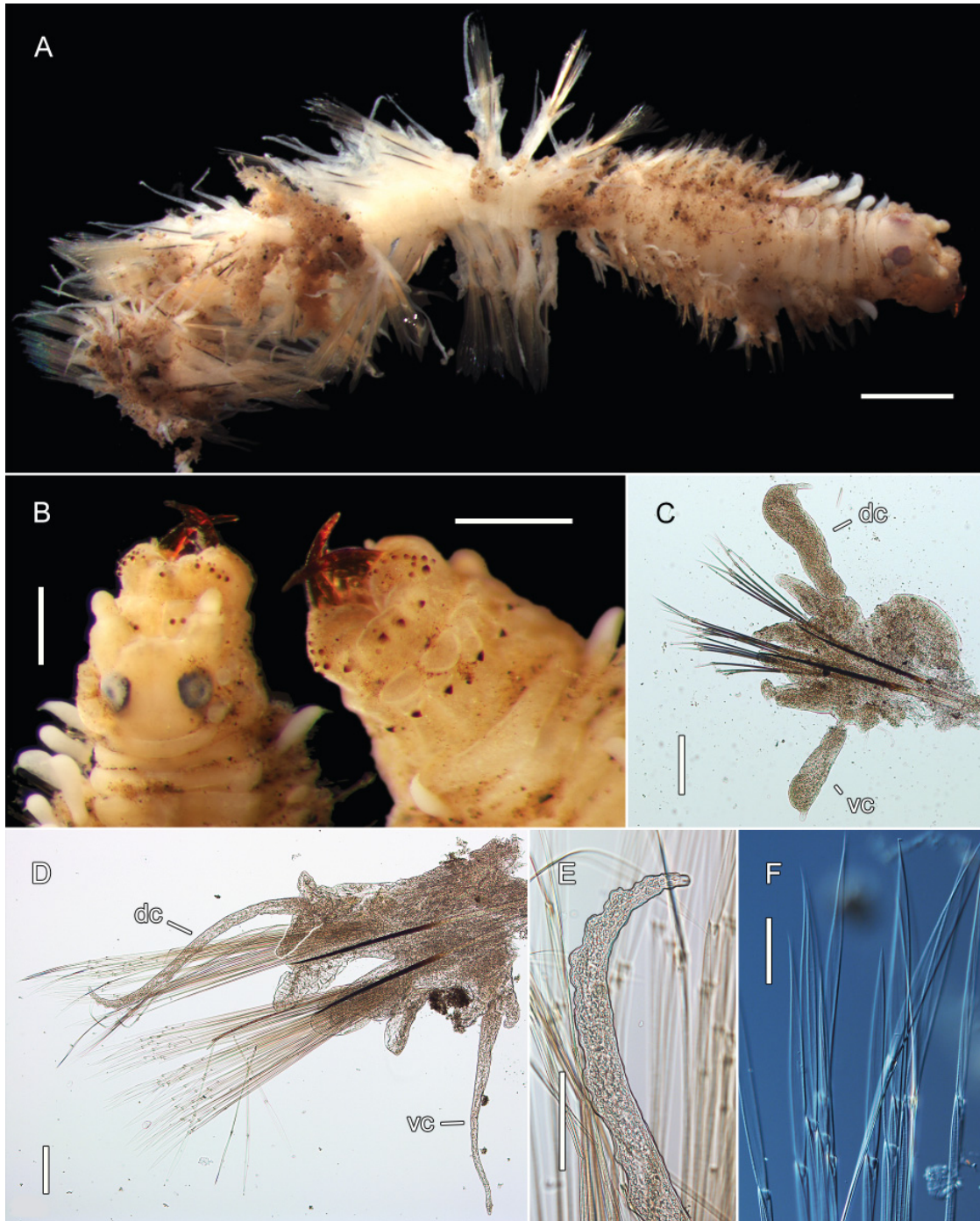


Fig. 6. *Neanthes goodayi* sp. nov., epitoke paratype (NHM_1783), preserved specimen. **A.** Entire specimen, dorsal view. **B.** Extruded pharynx, dorsal view (left), ventral view (right). **C.** Detail of pre-natatory parapodium 4, with modified dorsal and ventral cirri, posterior view. **D.** Detail of modified natatory swimming parapodium, chaetiger 31, posterior view. **E.** Detail of papillated dorsal cirrus, chaetiger 31, posterior view. **F.** Modified swimming spinigers, subacicular neurocheatal fascicle, chaetiger 32. Abbreviations: DC = dorsal cirrus; VC = ventral cirrus. Lobe at base of dorsal cirrus in D and E outlined with a fine white or black line. Parapodium in C dissected from left side of specimen; parapodium in D dissected from right side of specimen, with images D and E laterally inverted to follow direction of other plates. Scale bars: A = 1 mm; B = 500 μ m; C–D = 200 μ m; E = 100 μ m; F = 50 μ m.

with ensiform (knife-shaped) blades (Fig. 6F). No gametes observed, though the presence of slightly papillated dorsal cirri on natatory chaetigers suggests that this specimen is a male (Read 2007).

Juveniles

Several small, possibly juvenile specimens were observed; paratypes NHM_127, NHM_171, NHM_1254, TL = 1.0–2.5 mm, L15 = max. 2.2 mm, W15 = max. 0.2 mm, 10–18 chaetigers (Fig. 5A–D). Postero-dorsal tentacular cirri extending to chaetiger 6. Eyes poorly developed in these specimens, with anterior eye pair observed only as faintly pigmented crescents (Fig. 5B–D), lenses not obvious; posterior eye pair not visible in smallest specimens (Fig. 5C–D). The identity of these specimens was confirmed with genetic data. Due to their size and the delicate nature of specimens, pharyngeal and parapodial dissections were not conducted to preserve specimen integrity.

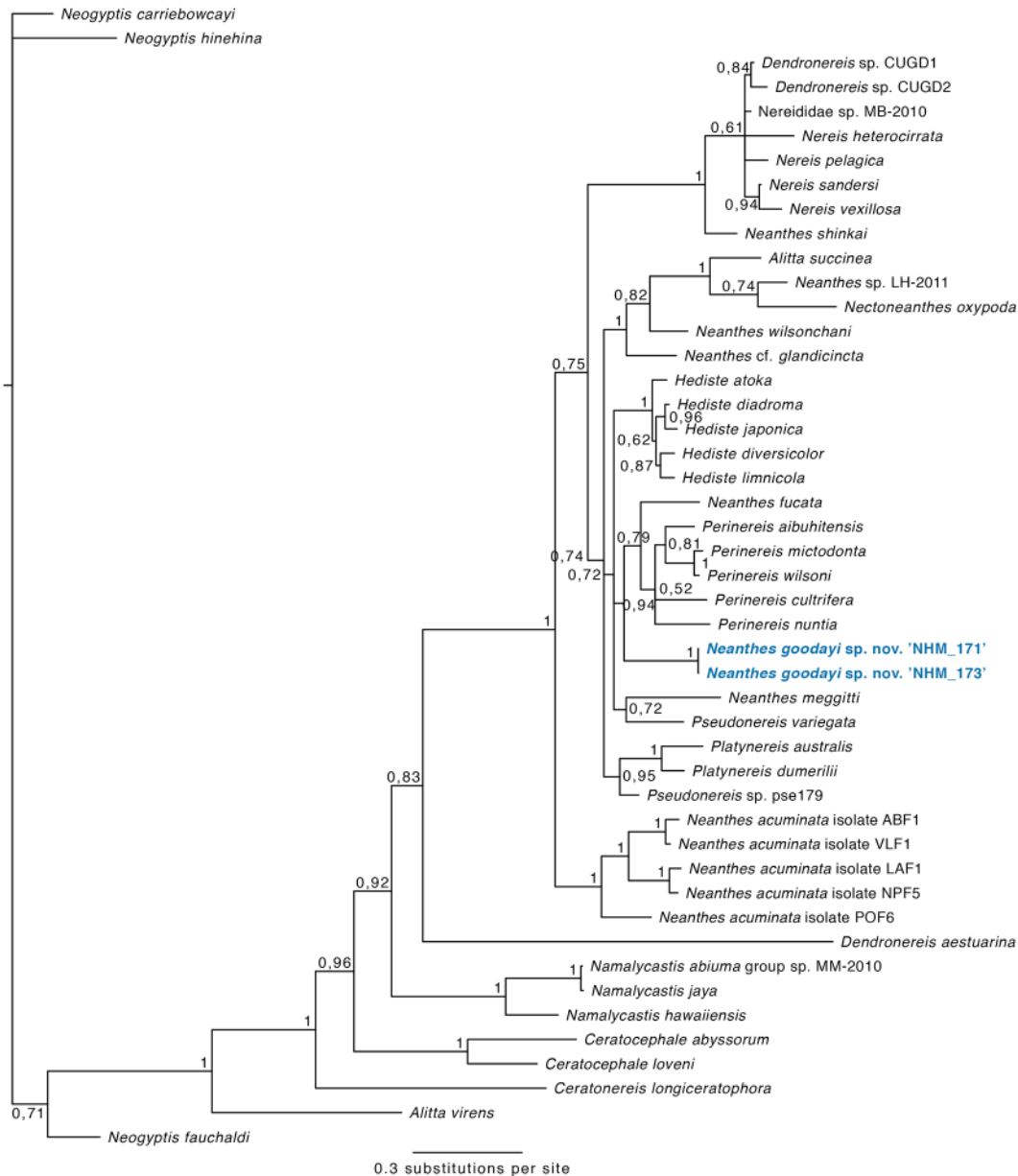


Fig. 7. Phylogenetic analysis of Nereididae Blainville, 1818, 50% majority rule tree from the Bayesian analyses using 18S, 16S and COI, with posterior probability values on nodes. Forty-five taxa from GenBank were included, using three taxa from another family within Nereidiformia, Hesionidae Grube, 1850, as outgroup.

Genetic data

All 43 individuals were sequenced for 16S and COI. The gene 16S was successfully sequenced in all but six specimens. COI sequencing was less successful; however, each specimen had coverage of at least one of the two genes. All specimens formed a single clade with low intraspecific divergence. Several specimens were also sequenced for 18S in order to assess deeper taxonomic relationships. This species was genetically distinct from all other species included in our phylogenetic analyses, and forms the basal branch of a clade including *Neanthes fucata* (Savigny, 1822) and five species of *Perinereis* Kinberg, 1865 (Fig. 7).

Remarks

This species is most consistent with the genus *Neanthes* Kinberg, 1865, most recently defined by Ibrahim *et al.* (2019). Previous analyses based on morphological parsimony suggested that neither of the three most species-rich nereidid genera, *Neanthes*, *Nereis* and *Perinereis*, can be considered monophyletic, with many generic characters displaying high homoplasy (Bakken & Wilson 2005). Molecular phylogenetic analyses carried out in this study supported the polyphyly of *Neanthes*, as sequences of species currently regarded as *Neanthes*, both from the ABYSSLINE material and from GenBank, rarely grouped together and were evenly distributed throughout a tree that included 11 other nereidid genera.

Neanthes goodayi sp. nov. can be differentiated from the majority of its congeners by the notably large anterior pair of eyes. Only *N. heteroculata* (Hartmann-Schröder, 1981), described from abyssal (4700 m) waters off the Bay of Biscay in the northeastern Atlantic, appears to possess comparably large anterior and minute posterior pairs of eyes. *Neanthes heteroculata* and *N. goodayi* sp. nov. also display similarities with regard to several other characters, such as the appearance of the prostomium, antennae and tentacular cirri, in addition to the types of chaetae present and their appearance and arrangement. Based on an examination of the type material of *N. heteroculata*, *N. goodayi* sp. nov. differs in having distinctly rounded, spherical to ovoid palpophores (e.g., Fig. 4B), with palpophores in *N. heteroculata* found to be narrower, bluntly conical in shape. Furthermore, the dorsal cirri are relatively short in *N. heteroculata*, not exceeding the length of the notopodial ligules, whereas they exceed the length of the notopodial ligules in at least anterior and posterior chaetigers in *N. goodayi* sp. nov.

Notably, *N. heteroculata* is one of a handful of species of *Neanthes* reported from the deep sea. Of the 84 currently valid species of *Neanthes* (Read & Fauchald 2020b) only 13 have been reported from depths greater than 200 m (Khlebovich 1996; Shimabukuro *et al.* 2017; Hsueh 2019). Of these, *N. goodayi* sp. nov. also resembles *N. papillosa* (Day, 1963), described from deep (2745 m) waters off Cape Town, South Africa. *Neanthes papillosa* similarly possesses an enlarged anterior pair of eyes relative to the posterior pair, in addition to long tentacular cirri, relatively elongate, conical parapodial ligules, and dorsal cirri that exceed the length of the notopodial ligules, becoming longer on posterior chaetigers. The holotype of *N. papillosa* is noted to have pale, poorly chitinised paragnaths, thus making them difficult to observe (Day 1963). However, despite having fewer paragnaths in number across all areas, they appear to be organised in similar arrangements as in *N. goodayi* sp. nov., such as a single row of paragnaths on areas VII–VIII (single row of large cones in *N. goodayi* sp. nov. with varying numbers of smaller cones laterally). However, *N. papillosa* can primarily be differentiated from *N. goodayi* sp. nov. in that the anterior pair of eyes does not appear to be as strikingly large as in *N. goodayi* sp. nov. or *N. heteroculata*; thus, there is less disparity between the anterior and posterior eye pairs in size. Additionally, *N. papillosa* can be further distinguished in that it does not bear homogomph falcigers and that parapodial lobes of midbody and posterior chaetigers bear numerous club-shaped papillae; however, it is worth considering that some characters of *N. papillosa* may be reproductive modifications, as the holotype is described from a single epikotous female specimen.

Neanthes goodayi sp. nov. also bears similarities to *N. vitiazi* Khlebovich, 1996 from abyssal waters (3342–4160 m) of southern Japan, primarily in terms of broadly similar paragnath distributions, bearing homogomph falcigers and in having a large anterior pair of eyes, which are illustrated as rings without strong pigment. *Neanthes vitiazi* differs in that it has long, digitate median ligules positioned at right angles to the notoacicula on midbody and posterior chaetigers. *Neanthes vitiazi* is also described as having brown pigmentation on parapodial appendages and dense spot-like pigmentation on the apodous anterior segment; *N. goodayi* sp. nov. similarly bears two pigmented spots on the dorso-lateral anterior margin of this segment; however, these are relatively small, whereas the spots in *Neanthes vitiazi* span much of the length of the segment and are placed dorsally, behind the eyes.

The geographically most proximal deep-water species, *N. mexicana* Fauchald, 1972, described from abyssal waters off Baja California, and *N. sandiegensis* Fauchald, 1977 from the San Diego Trough (728–855 m), can also be differentiated from *N. goodayi* sp. nov. *Neanthes mexicana* was originally described from a single damaged specimen, re-examined and revised by de León-González & Solís-Weiss (2000) with the addition of several nereidids collected from abyssal waters off California USA agreeing with the type specimen. *Neanthes mexicana* is described as bearing a single pair of very large red eyes, with diffuse pigment spots posterior to the eyes noted to perhaps represent the posterior eye pair (Fauchald 1972). In ABYSSLINE specimens, the appearance of the posterior eye pair was variable, ranging from discrete dark spots to more faint, irregular shapes, occasionally with one or both eyes absent all together, particularly in smaller specimens. The eye morphology of *N. mexicana* therefore falls within the variation observed in the ABYSSLINE samples. *Neanthes mexicana* and *N. goodayi* sp. nov. also share similarities in terms of parapodial morphology, with all parapodial ligules broadly conical to somewhat triangular in shape (see de León-González & Solís-Weiss 2000: fig. 3). However, *N. mexicana* differs from *N. goodayi* sp. nov. in terms of palp morphology (long, digitate palpostyles), the arrangement and number of paragnaths (4 cones in areas II and IV versus 12 cones in both areas in *N. goodayi* sp. nov.) and in lacking homogomph falcigers.

Neanthes sandiegensis is only known from a single damaged specimen. However, it differs from *N. goodayi* sp. nov. primarily in terms of parapodial morphology, bearing large, foliose dorsal notopodial ligules with medially inserted, long, flattened digitate dorsal cirri, long digitate prechaetal notopodial lobes and notably elongate ventral neuropodial ligules. *Neanthes sandiegensis* also differs in terms of the distribution and number of paragnaths on most pharyngeal areas (I = 0, II = 2, VI = 6–8, VII–VIII = 35 in *N. sandiegensis*, I = 2, II = 12, VI = 1–4, VIII–VIII = 19 in the holotype of *N. goodayi* sp. nov.).

While none of the morphologically most similar or geographically proximal congeners had genetic data available for comparison, morphological differences existed in each case. *Neanthes goodayi* sp. nov. can be differentiated from other deep-water *Neanthes* spp. primarily in terms of eye morphology: *N. articulata* Knox, 1960, *N. donggungensis* Hsueh, 2019, *N. kerguelensis* (McIntosh, 1885) and *N. suluensis* Kirkegaard, 1995 bear two relatively small, subequal eye pairs, whereas *N. bioculata* (Hartmann-Schröder, 1975) bears a single pair of small eyes; *N. abyssorum* Hartman 1967, *N. kermadeca* (Kirkegaard, 1995), *N. shinkai* Shimabukuro *et al.*, 2017 and *N. typhla* (Monro, 1930) are recorded as lacking eyes altogether and can be further differentiated from *N. goodayi* sp. nov. in terms of paragnath distribution, among other characters (see Shimabukuro *et al.* 2017 for comparative morphological table of most deep water *Neanthes* spp.).

Ecology

Neanthes goodayi sp. nov. was found at depths ranging from 4000 to 4400 m living in crevices of polymetallic nodules (Fig. 8A–B), burrowing in xenophyophore foraminifera growing on nodules (Fig. 8C–E) or in mud balls on nodule surfaces (Fig. 8F–H). As in other nereidids, the strong eversible jaws, together with large eyes, indicate an active and predatory behaviour. While we were able to

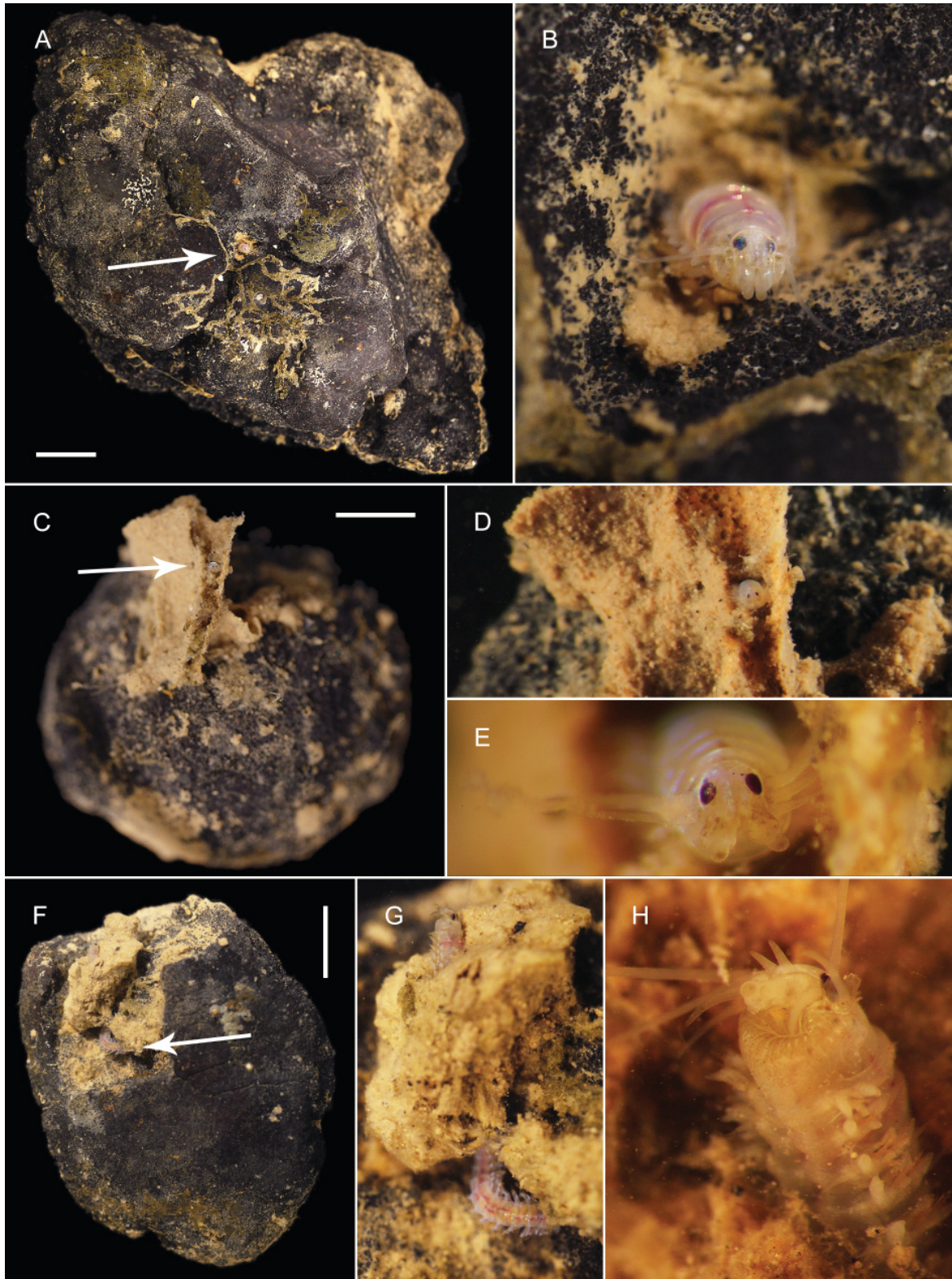


Fig. 8. *Neanthes goodayi* sp. nov., live specimens, in situ images. **A.** Paratype (NHM_2026), burrowing within nodule crevice. **B.** Detail of paratype (NHM_2026), in burrow. **C.** Paratype (NHM_512), burrowing within a foraminiferan growing on nodule. **D–E.** Detail of paratype (NHM_512), in burrow. **F.** Detail of paratype (NHM_1624), burrowing within a mudball encrusting the nodule surface. **G–H.** Details of paratype (NHM_1624), in burrow. Scale bars: 1 cm.

observe live, moving specimens kept at cold temperatures even after recovery from 4000 m water depth, behaviours such as predation were not observed. Polymetallic nodules are thought to contain a diverse meiofaunal community of nematodes, copepods and other small crustaceans; thus, it is possible that *N. goodayi* sp. nov. is a ‘sit and wait’ predator that is able to remain inside the nodules and detect prey passing overhead through extremely small variations in light (from local bioluminescence, detected by the large eyes) or other physio-chemical cues.

Distribution

Eastern Clarion Clipperton Fracture Zone, Central Eastern Pacific.

Discussion

It is perhaps remarkable that one of the more obvious and charismatic animals living on and inside the most investigated mineral resource on the deep seafloor has not been described until now. However, the CCZ region, despite a large number of expeditions and considerable sampling effort, has clearly never received appropriate taxonomic attention (Glover *et al.* 2018). Only in recent years has any effort been made to describe polychaete species, with 29 new species described in two recent papers (Bonafácio & Menot 2018; Wiklund *et al.* 2019). Such descriptions are essential to future investigations of population connectivity and resilience, extinction risk modelling, ecosystem function, natural history, ecology and life history (Glover *et al.* 2018).

The more obvious macrofauna that live on polymetallic nodules are likely to be useful in the future for monitoring the impacts of seabed mining, if it were to start. In this regard, *Neanthes goodayi* can be added to this list of potential ‘indicator taxa’ alongside the recently described nodule-dwelling sponge, *Plenaster craigi* Lim & Wiklund, 2017. Like *P. craigi*, *N. goodayi* sp. nov. is relatively easy to recognise during routine examination of nodules, and is sufficiently abundant to be counted in replicated samples. The smaller macrofauna dwelling in the sediments around the nodules is still extremely difficult to identify without using genetic methods and as such can only really be identified by specialists. The presence or absence of nodule-dwelling taxa such as *P. craigi* or *N. goodayi* sp. nov. may prove to be a useful measure of ecosystem health.

Acknowledgements

The UK Seabed Resources ABYSSLINE (ABYSSal baseLINE) environmental surveys were supported by a collaborative partnership between six non-profit global academic research institutes (University of Hawaii at Manoa, Natural History Museum, NORCE Norwegian Research Centre, National Oceanography Centre, Senckenberg Institute and Heriot-Watt University) and through an arrangement with UKSRL (UK Seabed Resources Ltd.). Additional support was provided by the Swedish research council FORMAS (TGD). We acknowledge Madeleine Brasier from the Natural History Museum team and Swee Cheng Lim from the National University of Singapore for support with sorting and sampling on board ship, and Chief Scientist Craig R. Smith for organizing the project and leading the sampling program. We also acknowledge the expert support from the Senckenberg Institute team in the deployment and recovery of successful Brenke epibenthic sledge samples. This study was made possible only by the dedicated help of the entire scientific party, the masters and crew of the RV *Melville* during the first cruise of the ABYSSLINE project in October 2013 and the masters and crew of the RV *Thomas G. Thompson* during the second ABYSSLINE cruise in February and March 2015. We sincerely thank reviewers for their effort in providing detailed comments and suggestions, which helped improve and clarify this manuscript. RD would like to thank and acknowledge support from the NERC INSPIRE DTP for the time needed to complete the manuscript. Thank you also to Emma Sherlock, Senior Curator of Annelida, Jackie Mackenzie-Dodds at the Molecular Collection Facility, and Harry Rousham and Robyn Fryer, Consultancy Group, all at the Natural History Museum.

References

- Amon D.J., Ziegler A.F., Dahlgren T.G., Glover A.G., Goineau A., Gooday A.J., Wiklund H. & Smith C.R. 2016. Insights into the abundance and diversity of abyssal megafauna in a polymetallic-nodule region in the eastern Clarion-Clipperton Zone. *Scientific Reports* 6: e30492. <https://doi.org/10.1038/srep30492>
- Bakken T. 2006. Redescription of two species of *Neanthes* (Polychaeta: Nereididae) possessing a large notopodial prechaetal lobe. *Scientia Marina* 70 (Suppl. 3): 27–33. <https://doi.org/10.3989/scimar.2006.70s327>
- Bakken T. & Wilson R.S. 2005. Phylogeny of nereidids (Polychaeta, Nereididae) with paragnaths. *Zoologica Scripta* 34 (5): 507–547. <https://doi.org/10.1111/j.1463-6409.2005.00200.x>
- Bely A.E. & Wray G.A. 2004. Molecular phylogeny of naidid worms (Annelida: Clitellata) based on cytochrome oxidase I. *Molecular Phylogenetics and Evolution* 30 (1): 50–63. [https://doi.org/10.1016/S1055-7903\(03\)00180-5](https://doi.org/10.1016/S1055-7903(03)00180-5)
- Bonifácio P. & Menot L. 2018. New genera and species from the Equatorial Pacific provide phylogenetic insights into deep-sea Polynoidae (Annelida). *Zoological Journal of the Linnean Society* 185 (3): 555–635. <https://doi.org/10.1093/zoolinnean/zly063>
- Cohen B.L., Gawthrop A. & Cavalier-Smith T. 1998. Molecular phylogeny of brachiopods and phoronids based on nuclear-encoded small subunit ribosomal RNA gene sequences. *Philosophical Transactions of the Royal Society of London B* 353 (1378): 2039–2061. <https://doi.org/10.1098/rstb.1998.0351>
- Dahlgren T.G., Lundberg J., Pleijel F. & Sundberg P. 2000. Morphological and molecular evidence of the phylogeny of nereidiform polychaetes (Annelida). *Journal of Zoological Systematics and Evolutionary Research* 38 (4): 249–253. <https://doi.org/10.1046/j.1439-0469.2000.384150.x>
- Day J.H. 1963. The polychaete fauna of South Africa. Part 8: new species and records from grab samples and dredgings. *Bulletin of the British Museum (Natural History), Series Zoology* 10 (7): 381–445.
- de León-González J.A. & Solís-Weiss V. 2000. A review of the polychaete family Nereididae from western Mexico. *Bulletin of Marine Science* 67 (1): 549–569.
- Droege G., Barker K., Seberg O., Coddington J., Benson E., Berendsohn W.G., Bunk B., Butler C., Cawsey E.M., Deck J., Döring M., Flemons P., Gemeinholzer B., Güntsch A., Hollowell T., Kelbert P., Kostadinov I., Kottmann R., Lawlor R.T., Lyal C., Mackenzie-Dodds J., Meyer C., Mulcahy D., Nussbeck S.Y., O'Tauma É., Orrell T., Petersen G., Robertson T., Söhngen C., Whitacre J., Wiczorek J., Yilmaz P., Zetzsche H., Zhang Y. & Zhou X. 2016. The Global Genome Biodiversity Network (GGBN) Data Standard specification. *Database* 2016: 1–11. <https://doi.org/10.1093/database/baw125>
- Edgar R.C. 2004. MUSCLE: multiple sequence alignment with high accuracy and high throughput. *Nucleic Acids Research* 32 (5): 1792–1797. <https://doi.org/10.1093/nar/gkh340>
- European Commission. 2020. Blue growth. Available from https://ec.europa.eu/maritimeaffairs/policy/blue_growth_en [accessed 17 Mar. 2020].
- Fauchald K. 1972. Benthic polychaetous annelids from deep water off western Mexico and adjacent areas in the eastern Pacific Ocean. *Allan Hancock Monographs in Marine Biology* 7: 1–575.
- Fauchald K. 1977. The polychaete worms. Definitions and keys to the orders, families and genera. *Natural History Museum of Los Angeles County, Science Series* 28: 1–188.
- Fauchald K. & Jumars P.A. 1979. The diet of worms: a study of polychaete feeding guilds. *Oceanography and Marine Biology Annual Review* 17: 193–284.

Folmer O., Black M., Hoeh W., Lutz R. & Vrijenhoek R. 1994. DNA primers for amplification of mitochondrial cytochrome c oxidase subunit I from diverse metazoan invertebrates. *Molecular Marine Biology Biotechnology* 3 (5): 294–299.

Glasby C.J., Wilson R.S. & Bakken T. 2011. Redescription of the Indo-Pacific polychaete *Neanthes pachychaeta* (Fauvel, 1918) n. comb. (Annelida, Phyllodocida, Nereididae) and its synonyms. *Zoosystema* 33 (3): 361–375. <https://doi.org/10.5252/z2011n3a5>

Glover A.G., Dahlgren T.G., Wiklund H., Mohrbeck I. & Smith C.R. 2016. An end-to-end DNA taxonomy methodology for benthic biodiversity survey in the Clarion-Clipperton Zone, Central Pacific abyss. *Journal of Marine Science and Engineering* 4 (1): e2. <https://doi.org/10.3390/jmse4010002>

Glover A.G., Wiklund H., Chen C. & Dahlgren T.G. 2018. Point of view: managing a sustainable deep-sea “blue economy” requires knowledge of what actually lives there. *eLife* 7: e41319. <https://doi.org/10.7554/eLife.41319>

Gooday A.J., Holzmann M., Caille C., Goineau A., Kamenskaya O., Weber A.A.T. & Pawlowski J. 2017. Giant protists (xenophyophores, Foraminifera) are exceptionally diverse in parts of the abyssal eastern Pacific licensed for polymetallic nodule exploration. *Biological Conservation* 207: 106–116. <https://doi.org/10.1016/j.biocon.2017.01.006>

Hartman O. 1954. Australian Nereidae including descriptions of three new species and one genus, together with summaries of previous records and keys to species. *Transactions of the Royal Society of South Australia* 77: 1–41.

Hein J.R., Mizell K., Koschinsky A. & Conrad T.A. 2013. Deep-ocean mineral deposits as a source of critical metals for high- and green-technology applications: comparison with land-based resources. *Ore Geology Reviews* 51: 1–14. <https://doi.org/10.1016/j.oregeorev.2012.12.001>

Hsueh P.W. 2019. *Neanthes* (Annelida: Nereididae) from Taiwanese waters, with description of seven new species and one new species record. *Zootaxa* 4554 (1): 173–198. <https://doi.org/10.11646/zootaxa.4554.1.5>

Ibrahim N.F., Ibrahim Y.S. & Sato M. 2019. New record of an estuarine polychaete, *Neanthes glandicincta* (Annelida, Nereididae) on the eastern coast of peninsular Malaysia. *ZooKeys* 831: 81–94. <https://doi.org/10.3897/zookeys.831.28588>

ISA. 2018. International Seabed Authority – Exploration Areas. Available from <https://www.isa.org.jm/contractors/exploration-areas> [accessed 12 Jul. 2021].

Jumars P.A., Dorgan K.M. & Lindsay S.M. 2015. Diet of Worms emended: an update of polychaete feeding guilds. *Annual Review of Marine Science* 7 (1): 497–520. <https://doi.org/10.1146/annurev-marine-010814-020007>

Katoh K. 2002. MAFFT: a novel method for rapid multiple sequence alignment based on fast Fourier transform. *Nucleic Acids Research* 30 (14): 3059–3066. <https://doi.org/10.1093/nar/gkf436>

Kearse M., Moir R., Wilson A., Stones-Havas S., Cheung M., Sturrock S., Buxton S., Cooper A., Markowitz S., Duran C. & Thierer T. 2012. Geneious Basic: an integrated and extendable desktop software platform for the organization and analysis of sequence data. *Bioinformatics* 28 (12):1647–1649. <https://doi.org/10.1093/bioinformatics/bts199>

Kersken D., Janussen D. & Martinez Arbizu P. 2019. Deep-sea glass sponges (Hexactinellida) from polymetallic nodule fields in the Clarion-Clipperton Fracture Zone (CCFZ), northeastern Pacific: Part II—Hexasterophora. *Marine Biodiversity* 49 (2): 947–987. <https://doi.org/10.1007/s12526-018-0880-y>

- Khlebovich V.V. 1996. Polychaetous Annelids, Volume III. Polychaetes of the family Nereididae of the Russian Seas and the adjacent waters. *Fauna of Russia and Neighbouring Countries* 140: 1–221.
- Kinberg J.G.H. 1865. Annulata nova. Nereidum dispositio nova. *Öfversigt af Kongelige Vetenskaps-akademiens Förhandlingar* 22: 167–179.
- Lim S-C., Wiklund H., Glover A.G., Dahlgren T.G. & Tan K-S. 2017. A new genus and species of abyssal sponge commonly encrusting polymetallic nodules in the Clarion-Clipperton Zone, East Pacific Ocean. *Systematics and Biodiversity* 15 (6): 507–519. <https://doi.org/10.1080/14772000.2017.1358218>
- Medlin L., Elwood H.J., Stickel S. & Sogin M.L. 1988. The characterization of enzymatically amplified eukaryotic 16S-like rRNA-coding regions. *Gene* 71 (2): 491–499. [https://doi.org/10.1016/0378-1119\(88\)90066-2](https://doi.org/10.1016/0378-1119(88)90066-2)
- Nygren A. & Sundberg P. 2003. Phylogeny and evolution of reproductive modes in Autolytinae (Syllidae, Annelida). *Molecular Phylogenetics and Evolution* 29 (2): 235–249. [https://doi.org/10.1016/S1055-7903\(03\)00095-2](https://doi.org/10.1016/S1055-7903(03)00095-2)
- Palumbi S.R. 1996. Nucleic acids II: the polymerase chain reaction. *Molecular Systematics* 2 (1): 205–247.
- Posada D. 2008. jModelTest: Phylogenetic model averaging. *Molecular Biology and Evolution* 25: 1253–1256. <https://doi.org/10.1093/molbev/msn083>
- Read G.B. 2007. Taxonomy of sympatric New Zealand species of *Platynereis*, with description of three new species additional to *P. australis* (Schmarda) (Annelida: Polychaeta: Nereididae). *Zootaxa* 1558 (1): 1–28. <https://doi.org/10.11646/zootaxa.1558.1.1>
- Read G. & Fauchald K. 2020a. World Polychaeta database. Nereididae Blainville, 1818. Available from <http://www.marinespecies.org/aphia.php?p=taxdetails&id=22496> [accessed 5 Feb. 2020].
- Read G. & Fauchald K. 2020b. World Polychaeta database. *Neanthes* Kinberg, 1865. Available from <http://www.marinespecies.org/aphia.php?p=taxdetails&id=129378> [accessed 5 Feb. 2020].
- Ronquist F., Teslenko M., Van Der Mark P., Ayres D.L., Darling A., Höhna S., Larget B., Liu L., Suchard M.A. & Huelsenbeck J.P. 2012. MrBayes 3.2: efficient Bayesian phylogenetic inference and model choice across a large model space. *Systematic Biology* 61 (3): 539–542. Retrieved from <https://doi.org/10.1093/sysbio/sys029>
- Sato M. 2013. Resurrection of the genus *Nectoneanthes* Imajima, 1972 (Nereididae: Polychaeta), with redescription of *Nectoneanthes oxypoda* (Marenzeller, 1879) and description of a new species, comparing them to *Neanthes succinea* (Leuckart, 1847). *Journal of Natural History* 47 (1–2): 1–50. <https://doi.org/10.1080/00222933.2012.743609>
- Shimabukuro M., Santos C.S.G., Alfaro-Lucas J.M., Fujiwara Y. & Sumida P.Y.G. 2017. A new eyeless species of *Neanthes* (Annelida: Nereididae) associated with a whale-fall community from the deep Southwest Atlantic Ocean. *Deep Sea Research II* 146: 27–34. <https://doi.org/10.1016/J.DSR2.2017.10.013>
- Sjölin E., Erséus C. & Källersjö M. 2005. Phylogeny of Tubificidae (Annelida, Clitellata) based on mitochondrial and nuclear sequence data. *Molecular Phylogenetics and Evolution* 35 (2): 431–441. <https://doi.org/10.1016/j.ympev.2004.12.018>
- Thiel H., Schriever G., Bussau C. & Borowski C. 1993. Manganese nodule crevice fauna. *Deep-Sea Research I* 40 (2): 419–423. [https://doi.org/10.1016/0967-0637\(93\)90012-R](https://doi.org/10.1016/0967-0637(93)90012-R)

Villalobos-Guerrero T.F. 2019. Redescription of two overlooked species of the *Perinereis nuntia* complex and morphological delimitation of *P. nuntia* (Savigny in Lamarck, 1818) from the Red Sea (Annelida, Nereididae). *Zoosystema* 41 (1): 465–496. <https://doi.org/10.5252/zoosystema2019v41a24>

Villalobos-Guerrero T.F. & Bakken T. 2018. Revision of the *Alitta virens* species complex (Annelida: Nereididae) from the North Pacific Ocean. *Zootaxa* 4483 (2): 1–257. <https://doi.org/10.11646/zootaxa.4483.2.1>

Weigert A. & Bleidorn C. 2016. Current status of annelid phylogeny. *Organisms Diversity and Evolution* 16 (2): 345–362. <https://doi.org/10.1007/s13127-016-0265-7>

Wieczorek J., Bloom D., Guralnick R., Blum S., Döring M., Giovanni R., Robertson T. & Vieglais D. 2012. Darwin Core: An evolving community-developed biodiversity data standard. *PLoS One* 7 (1): e29715. <https://doi.org/10.1371/journal.pone.0029715>

Wiklund H., Neal L., Glover A.G., Drennan R., Rabone M. & Dahlgren T.G. 2019. Abyssal fauna of polymetallic nodule exploration areas, eastern Clarion-Clipperton Zone, central Pacific Ocean: Annelida: Capitellidae, Opheliidae, Scalibregmatidae, and Traviidae. *ZooKeys* 883: 1–82. <https://doi.org/10.3897/zookeys.883.36193>

Wilson R.S. 1984. *Neanthes* (Polychaeta: Nereididae) from Victoria with descriptions of two new species. *Proceedings of the Royal Society of Victoria* 96 (4): 209–226.

Wilson R.S. 1988. Synonymy of the genus *Nectoneanthes* Imajima, 1972, with *Neanthes* Kinberg, 1866 (Polychaeta: Nereididae). *Proceedings of the Biological Society of Washington* 101 (1): 4–10.

Wu P., Sun J. & Yang T. 1985. *Nereidae (Polychaetous Annelids) of the Chinese Coast*. Springer-Verlag, Berlin, New York.

Manuscript received: 22 May 2020

Manuscript accepted: 8 June 2021

Published on: 27 July 2021

Topic editor: Rudy Jocqué

Desk editor: Danny Eibye-Jacobsen

Printed versions of all papers are also deposited in the libraries of the institutes that are members of the *EJT* consortium: Muséum national d'histoire naturelle, Paris, France; Meise Botanic Garden, Belgium; Royal Museum for Central Africa, Tervuren, Belgium; Royal Belgian Institute of Natural Sciences, Brussels, Belgium; Natural History Museum of Denmark, Copenhagen, Denmark; Naturalis Biodiversity Center, Leiden, the Netherlands; Museo Nacional de Ciencias Naturales-CSIC, Madrid, Spain; Real Jardín Botánico de Madrid CSIC, Spain; Zoological Research Museum Alexander Koenig, Bonn, Germany; National Museum, Prague, Czech Republic.

Supplementary file 1. DarwinCore Archive (DWcA) of all specimen occurrence (and associated preparation) data. <https://doi.org/10.5852/ejt.2021.760.1447.4755>